NASA TM X-53492

CRITICAL FLOWRATE OF TWO-PHASE NITROGEN

by HUGH M. CAMPBELL, JR. AND THOMAS J. OVERCAMP
Propulsion and Vehicle Engineering Laboratory

NASA

*George C. Marshall
Space Flight Center,
Huntsville, Alabama*

TECHNICAL MEMORANDUM X-53492

CRITICAL FLOWRATE OF TWO-PHASE NITROGEN

By

Hugh M. Campbell, Jr. and Thomas J. Overcamp

George C. Marshall Space Flight Center

Huntsville, Alabama

ABSTRACT

Experiments were done to learn the critical flowrate of two-phase nitrogen through an orifice. Recent analyses of the critical flowrate of a two-phase fluid are summarized and compared with experimental data. The experimental data appear to fit Ward's analysis better than any other analysis.

NASA - GEORGE C. MARSHALL SPACE FLIGHT CENTER

NASA-GEORGE C. MARSHALL SPACE FLIGHT CENTER

CRITICAL FLOWRATE OF TWO-PHASE NITROGEN

By

Hugh M. Campbell Jr. and Thomas J. Overcamp

APPLIED MECHANICAL RESEARCH BRANCH
PROPULSION DIVISION
PROPULSION AND VEHICLE ENGINEERING LABORATORY
RESEARCH AND DEVELOPMENT OPERATIONS

TABLE OF CONTENTS

PRECEDING PAGE BLANK NOT FILMED.

LIST OF ILLUSTRATIONS

DEFINITION OF SYMBOLS

Symbol	Definition	Units
A	Cross-Sectional Area	m^2
a, b, c, d, e	Parameters Defined in Equation (19)	-
h	Enthalpy	J/G
K	Slip Ratio Defined by Equation (13)	-
p	Pressure	N/cm^2
Q	Volumetric Flowrate	m^3/s
R	Gas Constant	$m^2/^0K\ kg\ s^2$
s	Entropy	J/G^0K
T	Temperature	^0K
v	Specific Volume	m^3/kg
v_m	Specific Volume Defined by Equation (2)	-
W	Weight (Mass) Flowrate	kg/s
x	Gravimetric Quality	-
y	Void Fraction or Volumetric Quality	-
Δh	Enthalpy of Vaporization	J/G
Δs	Entropy of Vaporization	J/G^0K
γ	Ratio of Specific Heats	-
ζ	Weight Flowrate per Unit Cross-Sectional Area	$kg/m^2\ s$
ψ	Fluid Velocity	m/s

DEFINITION OF SYMBOLS (Concluded)

SUBSCRIPTS

Symbol	Definition
g	Vapor State
ℓ	Liquid State
m	Maximum
o	Stagnation State
p	Pressure
s	Constant Entropy

CRITICAL FLOWRATE OF TWO-PHASE NITROGEN

By

Hugh M. Campbell, Jr. and Thomas J. Overcamp*

George C. Marshall Space Flight Center

SUMMARY

Experiments were done to determine the critical flowrate for two-phase nitrogen. Recent critical two-phase fluid flow analyses are summarized and compared with experimental results obtained in this program.

Most critical two-phase fluid flow analyses utilize an assumption of thermodynamic equilibrium, which causes experimental results to deviate from the analysis at low qualities. This characteristic deviation was noted in the data obtained during this program. The experimental data appear to be more closely approximated by Ward's analysis than any other.

INTRODUCTION

Since the end of World War II scientists have devoted much time to the investigation of two-phase fluid flow, critical two-phase fluid flow, and heat transfer to a two-phase fluid. The major portion of the work on two-phase fluid flow was for application to nuclear reactor design. Consequently most of the analyses were verified with water and steam. With the advent of space boosters, considerable curosity has been expressed over the critical two-phase flow for the cryogenic fluids. The investigation of two-phase fluid flow phenomena is important in answering questions on the venting of propellant tanks while in orbit, chill of transfer and engine propellant lines, and in advancing the state-of-the-art in booster design.

The critical flowrate of a fluid is not a new phenomenon, but is well known, both theoretically and experimentally, for a compressible fluid. The theory of critical gaseous fluid flow is developed in most thermodynamics and compressible fluid-flow textbooks. When a

---

*NASA summer student employee, Michigan State University, East Lansing, Michigan

gaseous fluid flows through a restriction, the weight flowrate is increased by decreasing the pressure downstream of the restriction, because the potential causing the fluid to flow is the pressure gradient. As the downstream pressure continues to decrease, the weight flowrate continues to increase until a limiting weight flowrate is attained. This limiting weight flowrate is attained when the fluid velocity in the throat of the restriction coincides with the speed of sound in the flowing fluid. Once the critical flowrate is attained, additional decreases in downstream pressure will produce no change in the weight flowrate. With a constant upstream pressure, the maximum ratio of the pressure upstream of the restriction to the pressure at the smallest cross-sectional area in the restriction is known as the critical pressure ratio. The relationship between weight flowrate and pressure ratio is shown in Figure 1. The upstream pressure can be increased when the pressure ratio is subcritical, and the only changes in weight flowrate will be due to changes in fluid density or changes in the speed of sound in the flowing fluid caused by the increased pressure.

Two-phase fluid flow exhibits the same critical flow phenomenon as gaseous fluid flow. Two-phase critical flow is not analyzed so readily as gaseous fluid flow, and consequently, it is not analyzed in the textbooks. Critical two-phase fluid flow analysis is greatly hindered by thermodynamic metastability. Analyses based on a completely homogeneous fluid in thermodynamic equilibrium yield results considerably below measured flowrates. Analyses based on thermodynamic equilibrium and the various two-phase fluid flow patterns yield good results in long tubes where no large amount of thermodynamic metastability exists. Analyses assuming no exchange of mass from one phase to the other are also used to predict the critical two-phase flowrate.

RECENT ANALYSIS OF CRITICAL TWO-PHASE FLUID FLOW

Levy [1] predicted the critical two-phase mass flowrate for steam and water. Assuming thermodynamic equilibrium, each phase can be represented by a unique mean velocity and no frictional or hydrostatic head losses. This analysis was based on a momentum exchange derived earlier by the same author.

Using the relation:

$$\zeta^2 = 10^4 \left(\frac{dp}{dv_m} \right)_s \tag{1}$$

The parameter V_m is given by:

$$v_m = \frac{v_g \, x^2}{y} + \frac{v_\ell \, (1-x)^2}{(1-y)} \tag{2}$$

Using the Bernoulli equation and the equation of continuity with the assumptions of no frictional or hydrostatic pressure losses, the gravimetric and volumetric quality can be related by:

$$x = \frac{y\,(1 - 2y) + y\,\{(1 - 2y)^2 + y\,[(2 v_g / v_\ell)\,(1 - y)^2 + y(1 - 2y)]\}^{1/2}}{[(2 v_g / v_\ell)\,(1 - y)^2 + y(1 - 2y)]} \tag{3}$$

Equation (3) is significant because it is an accurate relationship between gravimetric and volumetric quality that does not depend on the assumption of a homogeneous fluid, and nothing is required to relate these two parameters other than the liquid and vapor specific volume.

Equations (2) and (3) were then differentiated to give:

$$\left(\frac{\partial v_m}{\partial x}\right)_p = \frac{v_\ell\,(1 - x)^2 \left\{ 2\left[\dfrac{(1 - x)v_\ell}{(1 - y)}\right] - \dfrac{2\,x\,v_\ell}{y} - \dfrac{v_\ell(1 - x)}{(1 - y)^2} \right\}}{(1 - y)^3 \left[\dfrac{v_\ell(1 - x)^2}{(1 - y)^2} - \dfrac{x^2 v_g}{y^2} - \dfrac{v_\ell(1 - x)^2}{(1 - y)^3}\right]}$$

$$- \left[\frac{v_\ell\,(1 - x)}{(1 - y)^2}\right] \tag{4}$$

$$\left(\frac{\partial v_m}{\partial p}\right)_x = \frac{\left[\dfrac{v_\ell\,(1 - x)^2 \, x^2}{y}\right]\left[\left(\dfrac{v_g}{v_\ell}\right)\left(\dfrac{d v_g}{dp}\right) - \dfrac{d v_g}{dp}\right]}{(1 - y)^3 \left[\dfrac{v_\ell(1 - x)^2}{(1 - y)^2} - \dfrac{x^2 v_g}{y^2} - \dfrac{v_\ell(1 - x)^2}{(1 - y)^3}\right]}$$

$$+ 1/2 \left(\frac{d v_\ell}{dp}\right)\left[1 + \left(\frac{1 - x}{1 - y}\right)^2\right] \tag{5}$$

These results were then used in the following equation to determine $\left(\dfrac{d v_m}{dp}\right)_s$:

$$\left(\frac{dv_m}{dp}\right)_s = \left(\frac{\partial v_m}{\partial p}\right)_x - \left(\frac{\partial v_m}{\partial x}\right)_p \left[x\left(\frac{ds_g}{dp}\right) + (1-x)\left(\frac{ds_\ell}{dp}\right)\right]\left(\frac{1}{s_g - s_\ell}\right)$$

The results of equation (6) were used in equation (1) to determine the critical two-phase mass flowrate. This derivation assumes that the maximum critical two-phase flowrate is attained when the process through the obstruction is isentropic. Comparisons were made for an isenthalpic process and the difference between the values obtained using these two premises is small.

Comparison was made between the predicted values and experimental data from water and steam and the agreement was good. In all cases where Levy's prediction was compared with experimental data, the data were slightly below the predicted value or the prediction appeared to be a good average of the data. Critical throat pressure versus stagnation quality is shown for hydrogen in Figure 2, for nitrogen in Figure 4 and for oxygen in Figure 6 using Levy's analysis. Critical mass flowrate is shown versus stagnation quality for hydrogen in Figure 3, for nitrogen in Figure 5 and for oxygen in Figure 7 using Levy's analysis

Moody [2] predicted the maximum flowrate of a single component two-phase mixture assuming annular flow, uniform linear velocities for each phase, and thermodynamic equilibrium. He further assumed that the liquid and vapor were at the same static pressure at any axial location in the nozzle and that the slip ratio (the ratio of the mean vapor velocity to the mean liquid velocity) is an independant variable. Using the relations:

$$\zeta = \frac{W}{A} = \frac{y\,\psi_g}{x\,v_g} = \left(\frac{1-y}{1-x}\right)\frac{\psi_\ell}{v_\ell} \tag{7}$$

$$h_o = x\,(h_g + 10^{-3}\,\psi_g{}^2) + (1-x)\,(h_\ell + 10^{-3}\,\psi_\ell{}^2) \tag{8}$$

$$x = \frac{W_g}{W} \tag{9}$$

$$1-x = \frac{W_\ell}{W} \tag{10}$$

4

$$y = \frac{A_g}{A} \tag{11}$$

$$1-y = \frac{A_\ell}{A} \tag{12}$$

$$K = \frac{\psi_g}{\psi_\ell} \tag{13}$$

Equation (7), (8), (9), (10), (11), (12) and (13) can be solved to give the following relationship between x and y:

$$y = \frac{1}{1 + K\left[\left(\frac{1-x}{x}\right)\left(\frac{v_\ell}{v}\right)\right]} \tag{14}$$

By definition, the isentropic stagnation state is defined as, "the state a flowing fluid would attain if it underwent a reversibly adiabatic deceleration to zero velocity" [3]. Hence:

$$s_o = s = s_\ell + x\Delta s \tag{15}$$

Equations (7) through (15) were then solved to yield:

$$\zeta = \sqrt{\frac{10^3\left[(h_o - h_\ell) - \frac{\Delta h}{\Delta s}(s_o - s_\ell)\right]}{\left[\frac{s_g - s_o}{K^2\Delta s} + \frac{s_o - s_\ell}{\Delta s}\right]\left[(v_g/\Delta s)(s_o - s_\ell)\right] + \left[\left(\frac{K^2 v_\ell}{\Delta s}\right)(s_o - s_\ell)\right]^2}} \tag{16}$$

Equation (16) shows that the mass flowrate through a nozzle is a function of stagnation enthalpy, slip ratio, and pressure. Equation (16) was differentiated with respect to K and set equal to zero to yield:

$$K_m = \sqrt[3]{v_g/v_\ell} \tag{17}$$

and was differentiated with respect to pressure, set equal to zero, and the following equation resulted:

$$\zeta_m = \sqrt{2 \times 10^4\left[\frac{c}{a(ad + 2be)}\right]} \tag{18}$$

5

where:

$$a = K_m v_{\ell m} + x_m (v_{gm} - K_m v_{\ell m})$$

$$b = \frac{1}{K^2_m} + x_m \left(1 - \frac{1}{K^2_m}\right)$$

$$c = -[v_{\ell m} + x_m (v_{gm} - v_{\ell m})]$$

$$d = \left[\frac{1}{K^2_m(s_{gm} - s_{\ell m})}\right]\left(\frac{ds_g}{dp}\right)_m - \left(\frac{1}{s_{gm} - s_{\ell m}}\right)\left(\frac{ds_\ell}{dp}\right)_m$$

$$- \left[\frac{1}{K^4_m(s_{gm} - s_{\ell m})}\right]\left[\frac{d[K^2_m(s_{gm} - s_{\ell m})]}{dp}\right] \qquad (19)$$

$$+ x_m \left\{\left[\frac{1}{K^4_m(s_{gm} - s_{\ell m})}\right]\left[\frac{d K^2_m(s_g - s_\ell)}{dp}\right]_m\right.$$

$$\left. - \left(\frac{1}{s_{gm} - s_{\ell m}}\right)\left[\frac{d(s_g - s_\ell)}{dp}\right]_m\right\}$$

$$e = \left(\Delta s_m\right)\left[\frac{d}{dp}\left(\frac{K v_\ell}{\Delta s}\right)\right]_m + \left(\frac{K_m v_{\ell m}}{\Delta s_m}\right)\left(\frac{ds_g}{dp}\right)_m$$

$$- \left(\frac{v_{gm}}{\Delta s_m}\right)\left(\frac{ds_\ell}{dp}\right)_m + x_m\left\{\Delta s_m\left[\frac{d}{dp}\left(\frac{v_g}{\Delta s}\right)\right]_m - \Delta s_m\left[\frac{d}{dp}\left(\frac{K v_\ell}{\Delta s}\right)\right]_m\right\}$$

Curves were then presented showing the local pressure and maximum mass flowrates in terms of stagnation enthalpy and stagnation pressure. A comparison was made between the analysis and experimental data with a good degree of correlation. Critical throat pressure using Moody's Maximized Analysis is shown versus stagnation quality for hydrogen in Figure 8, for nitrogen in Figure 10, and for oxygen in Figure 12. Critical mass flowrate using Moody's Maximized Analysis is shown versus stagnation quality for hydrogen in Figure 9, for nitrogen in Figure 11, and for oxygen in Figure 13.

6

Ward [4] derived two models for predicting the critical two-phase mass flowrate. The following equations were used in both analyses.

$$x = \frac{W_g}{W} \tag{20}$$

$$A = A_\ell + A_g \tag{21}$$

$$\zeta_\ell = \frac{W_{\ell i}}{A_\ell} = \frac{\psi_\ell}{v_\ell} \tag{22}$$

$$\zeta_g = \frac{W_{gi}}{A_g} = \frac{\psi_g}{v_g} \tag{23}$$

Equations (20) through (23) were combined to yield:

$$\zeta = \frac{1}{\left[\frac{(1-x)}{\zeta_\ell} + \frac{x}{\zeta_g} \right]} \tag{24}$$

The following assumptions were utilized in the "Frozen Equilibrium Model":

1. No frictional pressure losses
2. No mass or energy exchange between the two phases
3. Isentropic expansion
4. Uniform pressures across any cross section
5. No shearing stress between the liquid and vapor phase
6. Negligible velocity at the orifice or nozzle inlet
7. The vapor phase behaves as a perfect gas

The liquid and vapor velocities may then be expressed as:

$$\psi_\ell = \sqrt{10^4 (p_o - p) v_\ell} \tag{25}$$

$$\psi_g = \sqrt{2 \times 10^4 R T_o \left(\frac{\gamma}{\gamma - 1} \right) \left[1 - \left(\frac{p}{p_o} \right)^{(\gamma - 1)/\gamma} \right]} \tag{26}$$

Equations (25) and (26) can then be combined with the continuity equation to yield:

$$\zeta_\ell = \frac{W_{\ell o}}{A_\ell} = \frac{\psi_\ell}{v_\ell} = \sqrt{\frac{2 \times 10^4 (p_o - p)}{v_\ell}} \qquad (27)$$

$$\zeta_g = \frac{W_g}{A_g} = \frac{\psi_g}{v_g}$$

$$= \sqrt{\left(\frac{2 \times 10^4}{RT}\right)\left(\frac{\gamma}{\gamma - 1}\right)\left[1 - \left(\frac{p}{p_o}\right)^{\gamma - 1/\gamma}\right]}\left[p_o\left(\frac{p}{p_o}\right)^{1/\gamma}\right] \qquad (28)$$

Equations (27) and (28) were substituted into equation (24), differentiated with respect to (p / p_i), and equated to zero to yield:

$$\frac{d\zeta}{d(p/p_o)} = \left[\left(\frac{1 - x_o}{x_o}\right)\left(\frac{v_{\ell o}}{v_{g o}}\right)^{0.5}\right] \qquad (29)$$

$$- \frac{\left[1 - (p_t/p_o)\right]^{1.5}\left(\frac{\gamma + 1}{\gamma}\right)\left[\left(\frac{2}{\gamma + 1}\right)(p_t/p_o)^{(2-\gamma)/\gamma} - (p_t/p_o)^{1/\gamma}\right]}{\left(\frac{\gamma}{\gamma - 1}\right)^{0.5}\left[(p_t/p_o)^{2/\gamma} - (p_t/p_o)^{(\gamma + 1)/\gamma}\right]^{1.5}} \equiv 0$$

The ratio of throat pressure to inlet pressure that would satisfy equation (29) was then determined for several values of the specific heat ratio and inlet pressure. These values of the ratio of throat pressure to inlet pressure were then used in equations (24), (27) and (28) to compute the critical two-phase mass flowrate. Critical throat pressure versus stagnation quality using Ward's Frozen Equilibrium Model is shown for hydrogen in Figure 14, for nitrogen in Figure 16 and for oxygen in Figure 18. Critical mass flowrate versus stagnation quality is shown for hydrogen in Figure 15, for nitrogen in Figure 17 and for oxygen in Figure 19.

The following assumptions were used with the Separate-Phase Shifting Equilibrium Model:

1. No frictional pressure losses
2. No mass or energy exchange between the two phases

8

3. Thermodynamic equilibrium

4. Isentropic expansion

5. The portion of the liquid which vaporizes or gas that condenses continues to move at the same velocity as its parent phase.

6. The static pressure is uniform across any cross section

7. Negligible velocity at the nozzle or orifice inlet

From the general energy equation, the liquid and gas velocity can be expressed as:

$$\psi_\ell = \sqrt{2 \times 10^4 (h_{\ell o} - h_\ell)} \tag{30}$$

$$\psi_g = \sqrt{2 \times 10^4 (h_{go} - h_g)} \tag{31}$$

Combining equations (30) and (31) with the continuity equation and substituting this result into equation (24) yields:

$$\zeta = \cfrac{1}{\left[\cfrac{(1 - x_i) v_\ell}{\sqrt{2 \times 10^4 (h_{\ell o} - h_\ell)}} + \cfrac{x_i v_g}{\sqrt{2 \times 10^4 (h_{go} - h_g)}} \right]} \tag{32}$$

Assuming a constant inlet pressure and quality, then allowing the downstream pressure to decrease, equation (32) will attain a maximum and thereafter will decrease. This maximum point is the maximum flowrate obtained by the "Separate-Phase Shifting Equilibrium Model."

Critical throat pressure versus stagnation quality using this analysis is shown for hydrogen on Figure 20, for nitrogen on Figure 22, and for oxygen on Figure 24. Critical mass flowrate versus stagnation quality is shown on Figure 21 for hydrogen, for nitrogen on Figure 23, and for oxygen on Figure 25.

USE OF CURVES

Using Figure 2 through 25, the critical pressure and mass flowrate may be read directly. The charts using the desired model and fluid are first determined. The stagnation quality and pressure

are entered, and the critical throat or receiver pressure is determined. Any absolute receiver pressure below the critical pressure will not alter the mass flowrate. Any absolute receiver pressure above the critical pressure will result in sub-critical fluid flow, and the flowrate can be determined using various equations for two-phase fluid flow through a restriction.

The stagnation quality and pressure are then entered into the charts to determine the critical mass flowrate. The critical mass flowrate will be unique when the receiver pressure is below or equal to the critical pressure.

EXPERIMENTAL APPARATUS AND PROCEDURE

Experimental Apparatus

The experimental apparatus consisted of a 4.7 cm (1.87 in.) diameter by 86.5 cm (34 in.) long horizontal, cylindrical plenum chamber. The two-phase fluid entered the plenum through a 1.06 cm (0.42 in.) diameter square-edge orifice and exited through a 2.87 cm (1.13 in.) diameter square-edge orifice.

Two-phase fluid flow was generated upstream of the plenum by mixing liquid and gaseous nitrogen. Slightly subcooled liquid nitrogen was supplied to the region immediately upstream of the plenum from a liquid nitrogen Dewar. Liquid flowrate was measured with a turbine-type flowmeter. Liquid nitrogen temperature was measured with a copper-constantan thermocouple. Gaseous nitrogen from a high pressure GN_2 supply system was supplied to the region immediately upstream of the plenum where it was mixed with LN_2 to give the two-phase fluid with the desired quality. GN_2 flowrate was measured with a turbine-type flowmeter, temperature was measured with a copper-constantan thermocouple, and pressure was measured with a pressure gauge. The plenum chamber and mixing region were insulated with polyurethane foam to prevent heat transfer to the fluid.

The two-phase fluid was exhausted from the plenum chamber through the 2.87 cm diameter orifice into a vacuum chamber.

A schematic of the experimental apparatus is shown in Figure 26, and the apparatus is pictured in Figure 27.

10

Experimental Procedure

Upon starting an experiment, liquid and gaseous nitrogen were mixed in such proportions as to give the desired quality. Fluid was then allowed to flow through the mixing region and plenum chamber into the vacuum chamber until the apparatus had reached thermal equilibrium. After sufficient time was allowed for the apparatus to reach thermal equilibrium, the data were recorded.

To insure critical flow through the upstream orifice, the plenum chamber pressure was maintained below 2.85 N/cm^2 (4.0 psia). Experimental conditions were selected so that the entire quality range was covered.

Data Reduction

Volumetric flowrates were converted to mass flowrates using fluid properties tabulated in Reference 5 . Knowing the mass flowrates and fluid states, and assuming:

1. Negligible fluid kinetic energy
2. No heat transfer to the fluid

the fluid quality can be computed by the following equation.

$$x_o = \frac{W_v h_{vo} + W_\ell h_{\ell o}}{\Delta h_o (W_{vo} + W_{\ell o})} - \frac{h_{\ell o}}{\Delta h_o} \tag{33}$$

Results

Thirty-six experiments were conducted that covered the entire quality range. Experimental results are tabulated in Table I and are plotted versus stagnation quality in Figure 28.

Experimental data are compared to the predictions in Figure 28. The experimental data were divided by 0.6 to account for the effect of the orifice coefficient.

CONCLUSIONS

Upon comparing the analytical predictions to the experimental data, it can be concluded that the analytical predictions are valid for the cryogens. After adjusting the experimental data to compensate for the orifice coefficient, it can be seen that the experimental data are best approximated at high quality by Ward's Separate Phase Shifting Equilibrium Model, and at low qualities by Moody's Analysis. The shape of the experimental data, when plotted versus stagnation quality, is best approximated by Ward's Frozen Equilibrium Model.

It should be noted that the predictions are valid for a medium to high-quality fluid, but fail for a low-quality fluid.

REFERENCES

1. Levy, S., Prediction of Two-Phase Critical Flow Rate, Journal of Heat Transfer, Vol C87, No. 1, pp 53-58, February 1965.

2. Moody, F. J., Maximum Flowrate of a Single Component, Two-Phase Mixture, Journal of Heat Transfer, Vol C87, No. 1, pp 134-142, February 1965.

3. Van Wylen, Gorden J., Thermodynamics, p 343, second edition, John Wiley and Sons, New York, N. Y., 1962.

4. Ward, Wiley, D., Calculations of Mass-Flow and Thrust Produced for a Two-Phase Fluid Mixture Passing Through a Choked Nozzle, NASA Technical Memorandum No. TMX-53269, George C. Marshall Space Flight Center, August 4, 1965.

5. Strobridge, Thomas R, The Thermodynamic Properties of Nitrogen From 114 to 540 R between 1.0 and 3000 psia, Supplement A (British Units)., National Bureau of Standards, Technical Note 129A, February 1963.

BIBLIOGRAPHY

Binder, R. C., Fluid Mechanics third ed., Prentice-Hall Inc., Englewood Cliff, N. J., 1956.

Stewart, R. B., Hust, J. G., and McCarty, R. D., Interim Thermodynamic Properties for Gaseous Oxygen at Temperatures From 55 to 300K and Pressures to 300 Atmospheres, National Bureau of Standards Report No. 7922, October 1963.

Dean, John W., A Tabulation of The Thermodynamic Properties of Normal Hydrogen Form Low Temperature to 540 R and From 10 to 1500 psia, Supplement A (British Units), National Bureau of Standards Technical Note 120A, June 1962.

TABLE I

EXPERIMENTAL RESULTS

Experiment No.	Q_ℓ (m³/s)	Q_g (m³/s)	GN_2 Temp (°K)	W (kg/s)	Quality x_0	P_2 (N/cm²)	P_3 (N/cm²)	P_4 (N/cm²)
1	.004558	.5863	272.22	.080	.477	17.024	2.241	1.469
2	.001699	.6160	267.77	.043	.969	16.962	2.186	1.469
3	.004360	.60923	268.33	.078	.511	17.265	2.227	1.0411
4	.002378	.6231	268.88	.052	.799	17.106	2.317	1.731
5	.005747	.5475	267.77	.094	.369	16.762	2.227	1.496
6	.004756	.5772	267.77	.083	.456	17.106	2.186	1.331
7	.003171	.5911	267.77	.062	.639	16.893	2.255	1.641
8	.001982	.60815	265.55	.047	.877	17.106	2.358	1.800
9	.004869	.5520	266.66	.083	.431	17.024	2.310	1.731
10	.004869	.5602	266.66	.083	.436	17.024	2.427	1.531
11	.002180	.5738	266.66	.049	.801	17.148	2.358	1.827
12	.002293	.5716	267.77	.050	.777	16.824	2.158	1.331
13	.002491	.5682	267.77	.052	.733	16.962	2.241	1.627
14	.002378	.5682	268.88	.051	.754	17.024	2.172	1.282
15	.005747	.4960	270.00	.094	.337	16.955	2.462	2.000
16	.007247	.6540	270.00	.117	.351	16.755	2.400	1.731
17	.002689	.5682	271.11	.055	.697	17.106	2.358	1.972
18	.005152	.5419	271.11	.086	.402	16.755	2.344	2.000
19	.008238	.1829	272.22	.114	.062	16.893	2.310	1.469
20	.004360	.5900	271.11	.077	.497	17.106	2.372	1.813
21	.008238	.4617	270.00	.124	.219	16.824	2.344	1.400
22	.013815	.5648	270.00	.092	.391	17.175	2.213	1.069
23	.003652	.6002	272.22	.069	.577	16.824	2.331	1.731
24	.002576	.6092	272.22	.055	.749	17.106	2.186	1.386
25	.003878	.5761	270.00	.071	.537	16.962	2.144	1.800
26	.004756	.5738	268.88	.082	.452	17.024	2.317	1.117
27	.003680	.5852	270.00	.068	.566	16.893	2.400	1.869
28	.007729	.4275	271.11	.101	.216	16.824	2.227	1.331
29	.006653	.4892	271.11	.104	.289	16.824	2.186	0.903
30	.010333	.3018	271.11	.146	.101	16.893	2.517	1.331
31	.00914	.4459	269.44	.135	.189	17.024	2.413	1.469
32	.00951	.1704	270.00	.131	.045	16.824	2.234	1.469
33	.010729	.2239	268.88	.148	.061	16.755	2.482	1.200
34	.01042	.27206	269.44	.146	.086	17.106	2.475	1.331
35	.008635	.3808	268.88	.126	.169	16.962	2.317	0.931
36	.012598	.1223	268.88	.169	.004	17.106	2.613	1.593
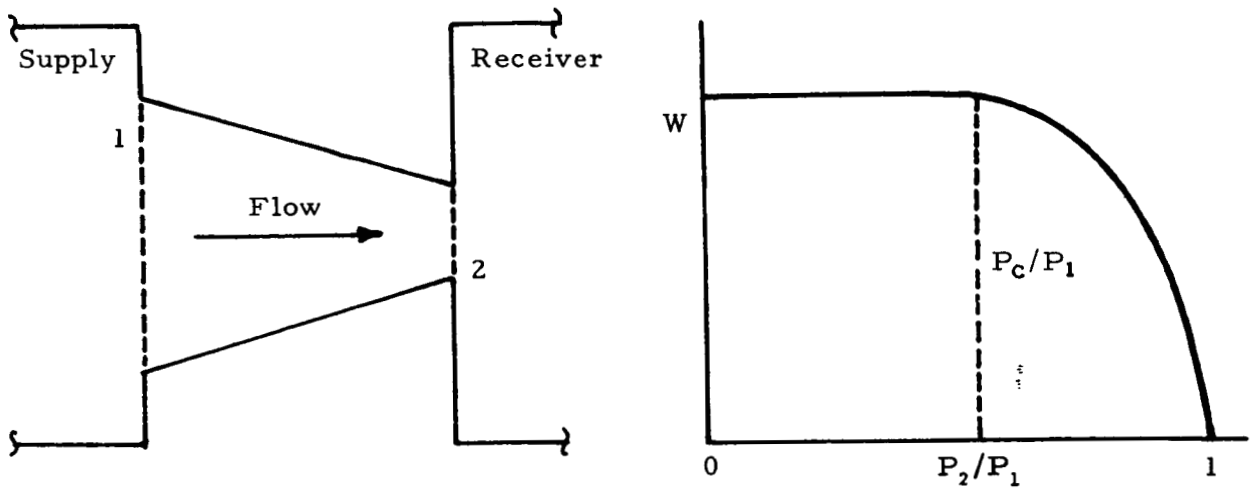
FIG 1   Relationship of Weight Flowrate Versus Pressure
for Compressible Fluid Flow
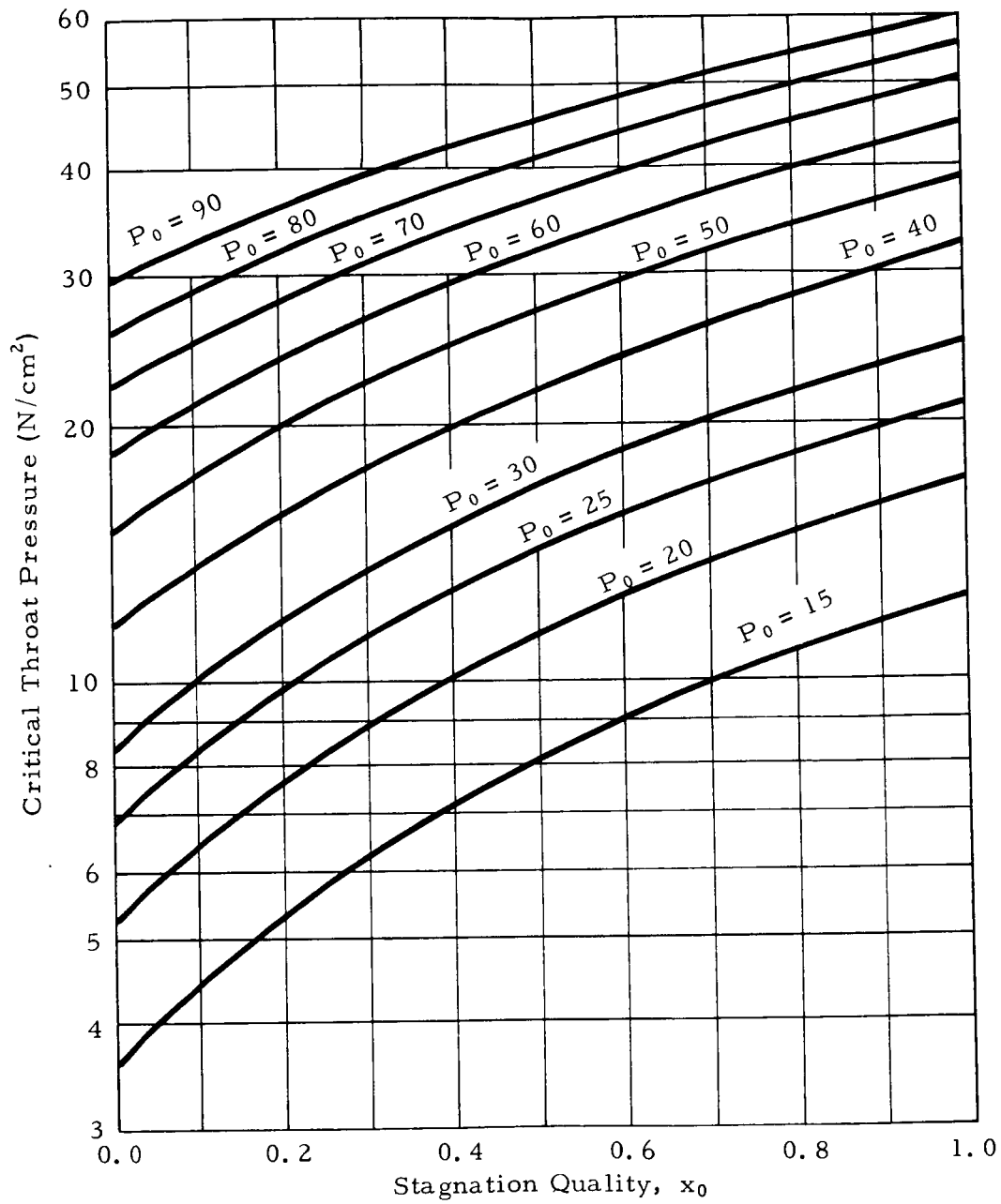
FIG 2   Critical Throat Pressure Versus Stagnation Quality
for Hydrogen (Levy's Momentum Exchange Analysis)

16

FIG 3   Critical Mass Flowrate Versus Stagnation Quality
         for Hydrogen (Levy's Momentum Exchange Analysis)

Critical Throat Pressure (N/cm^2)

Stagnation Quality, x_0

$P_0 = 250$

$P_0 = 200$

$P_0 = 150$

$P_0 = 100$

$P_0 = 75$

$P_0 = 50$

$P_0 = 25$
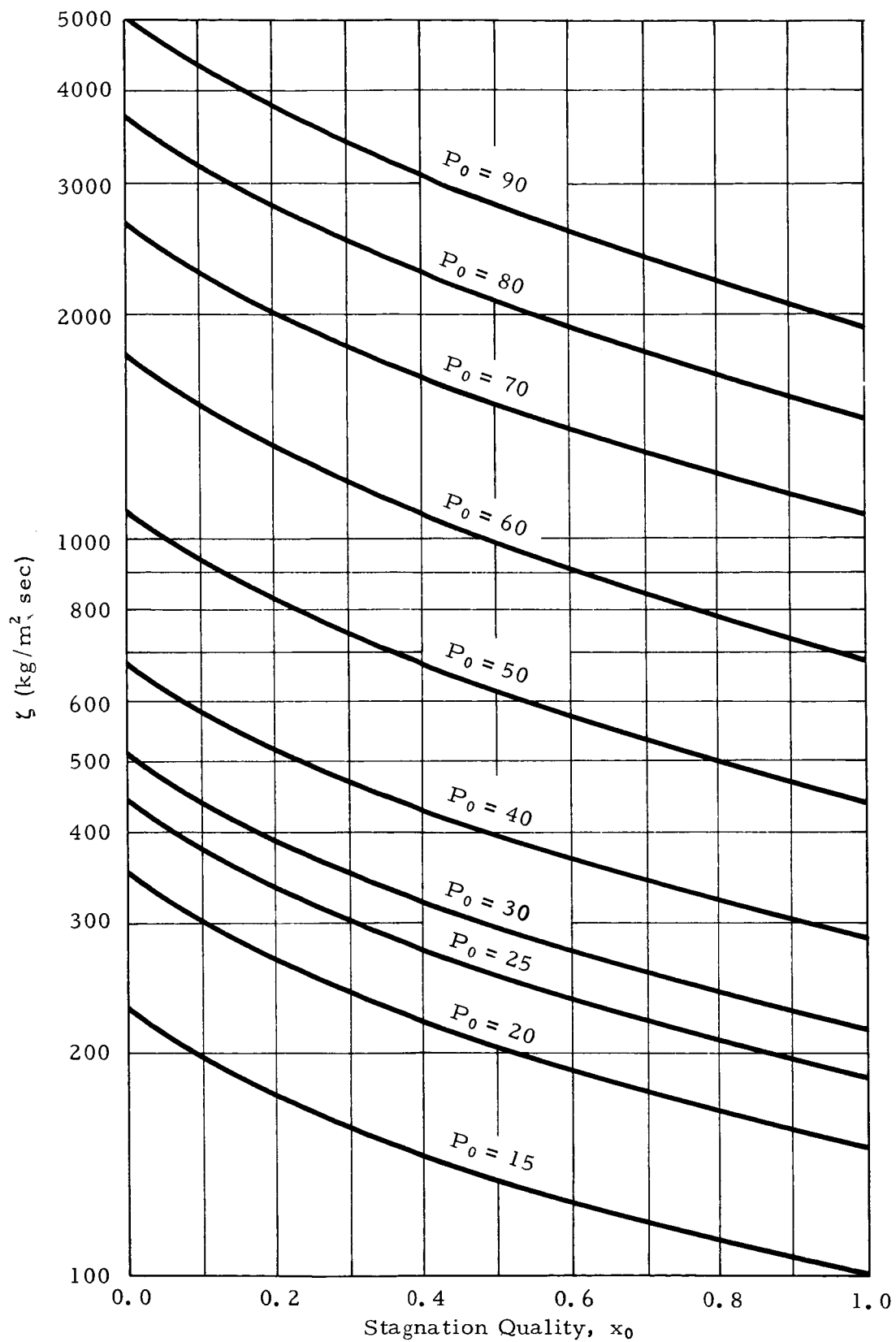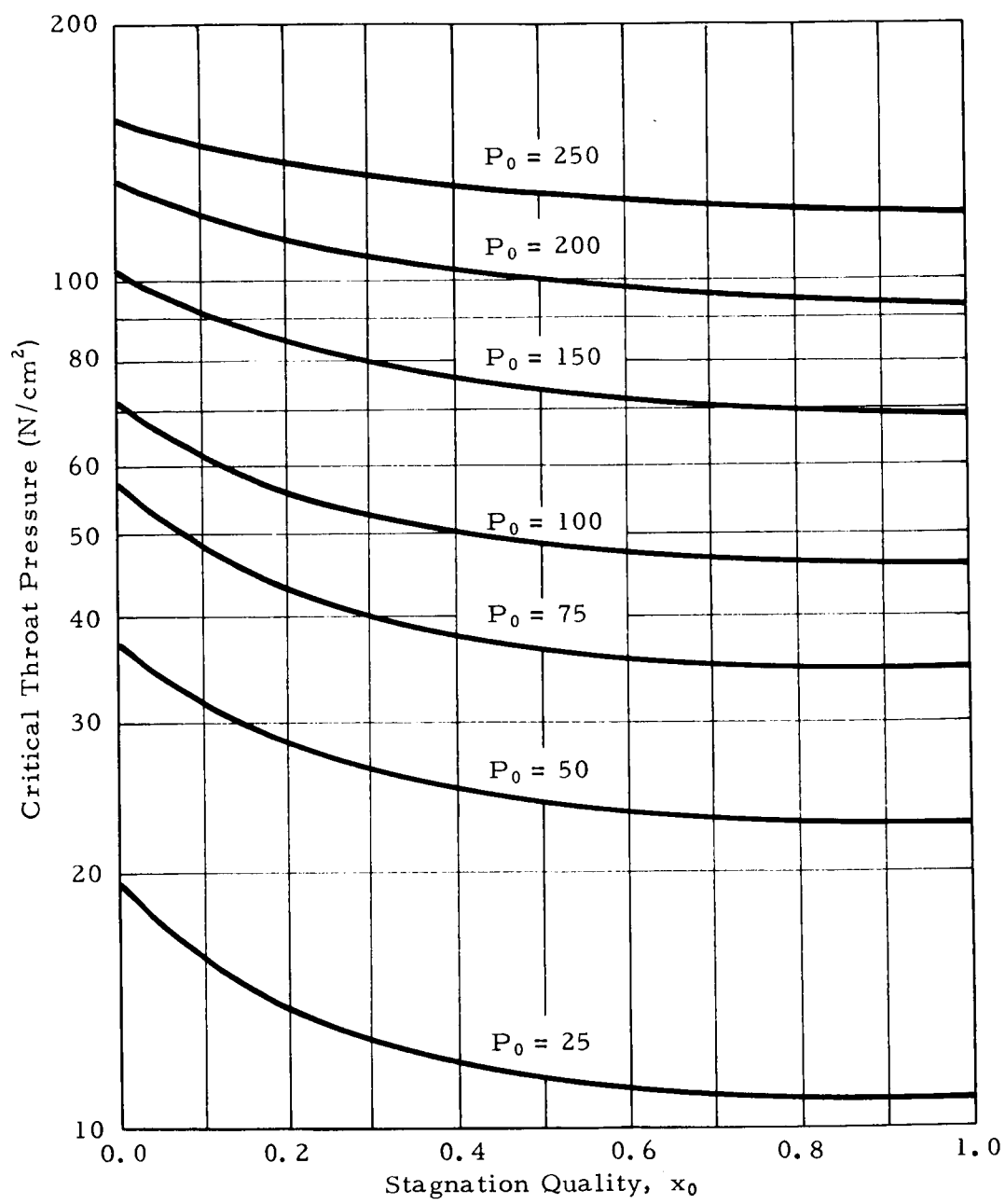
FIG 4   Critical Throat Pressure Versus Stagnation Quality for Nitrogen (Levy's Momentum Exchange Analysis)

18
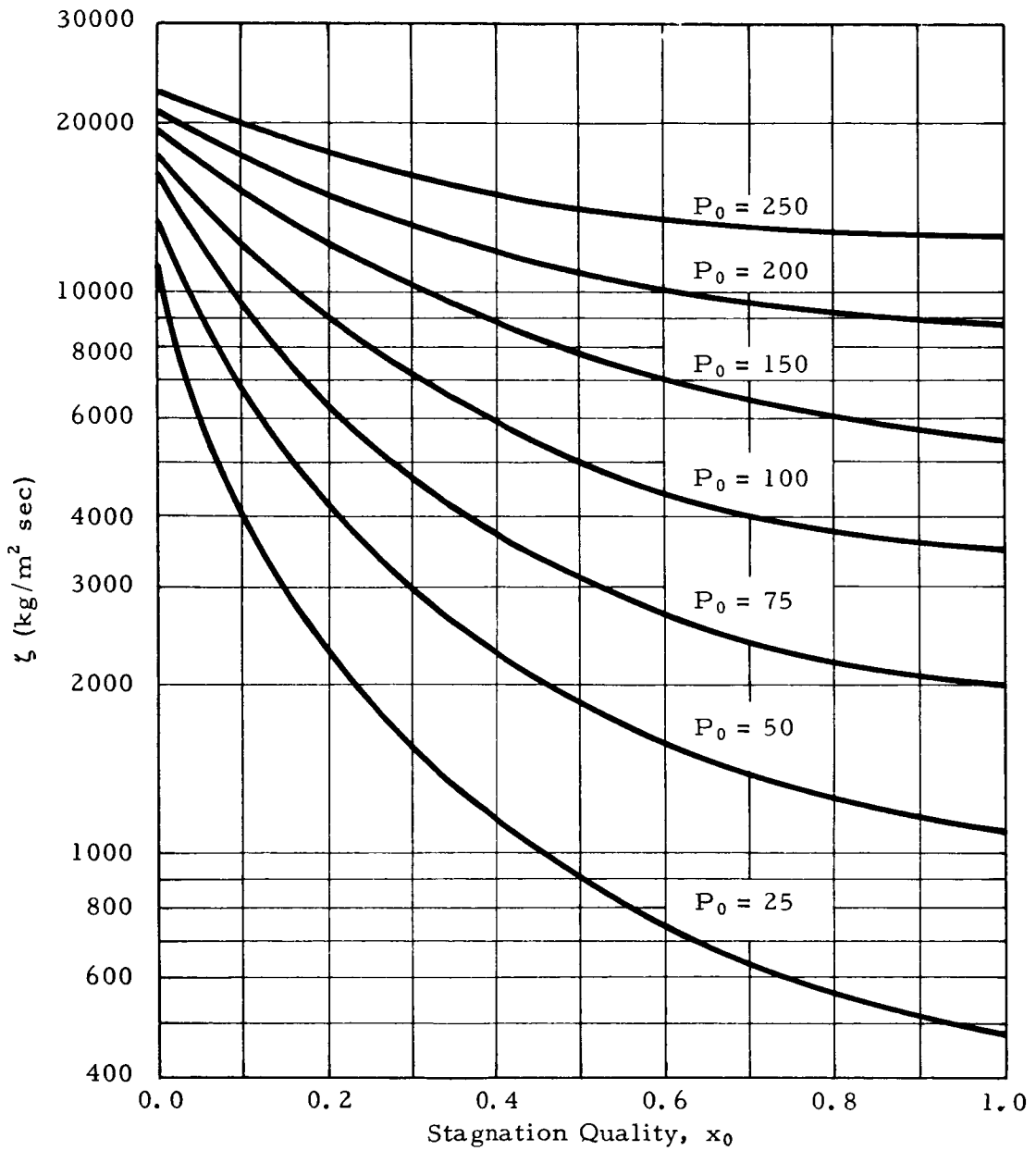
FIG 5   Critical Mass Flowrate Versus Stagnation Quality for
Nitrogen (Levy's Momentum Exchange Analysis)
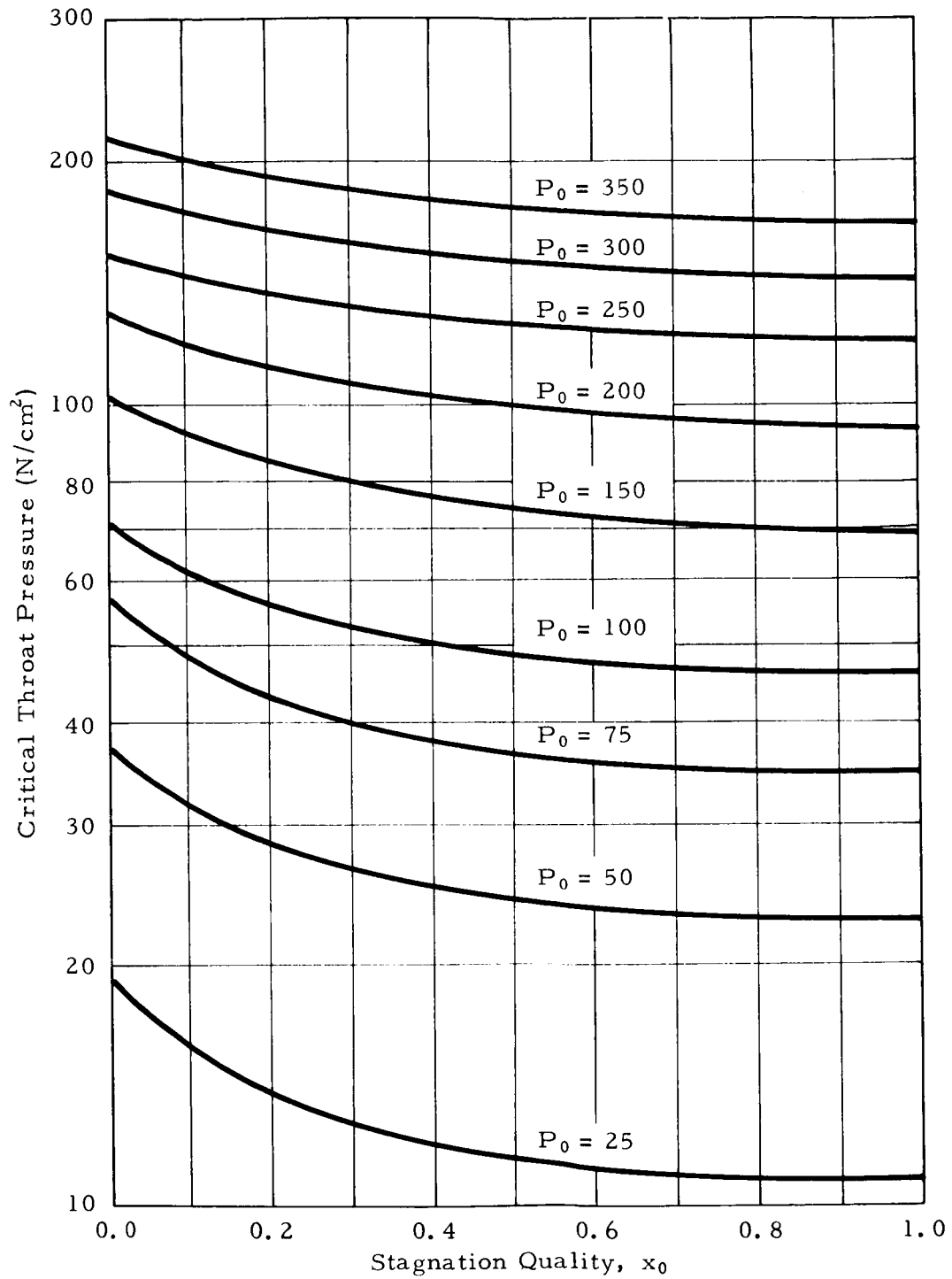
FIG 6   Critical Throat Pressure Versus Stagnation Quality
for Oxygen (Levy's Momentum Exchange Analysis)

20
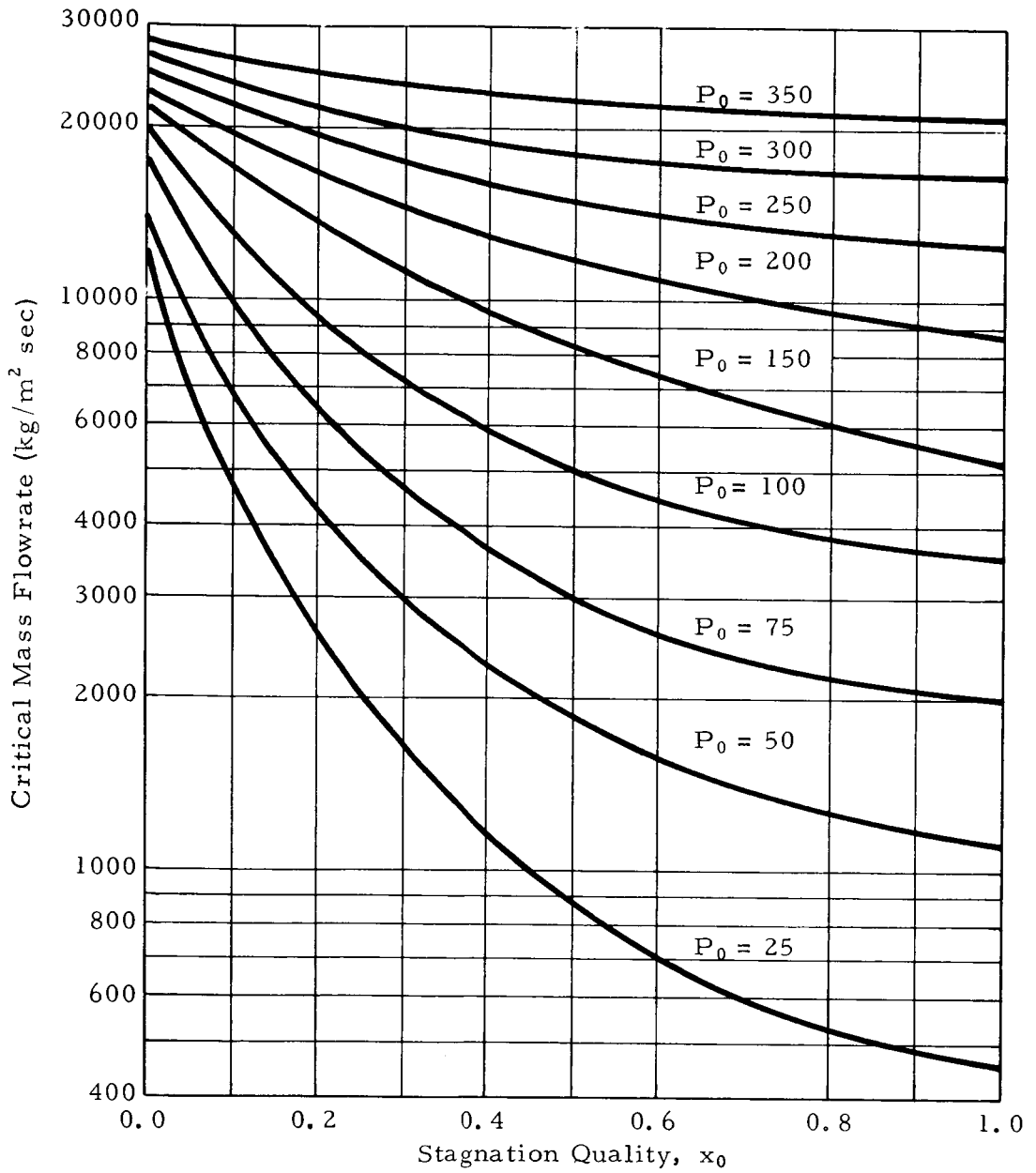
FIG 7   Critical Mass Flowrate Versus Stagnation Quality
         for Oxygen (Levy's Momentum Exchange Analysis)
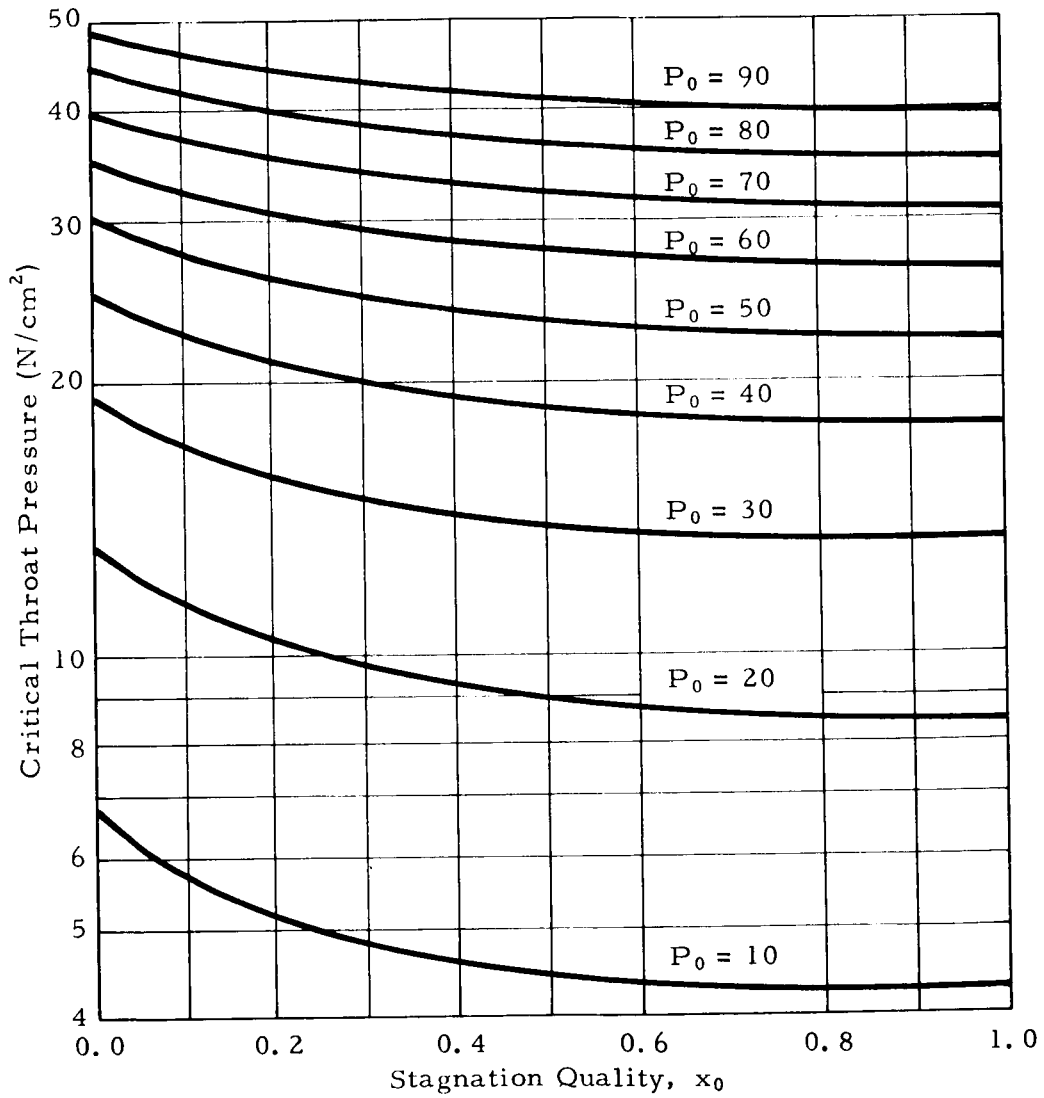
FIG 8   Critical Throat Pressure Versus Stagnation Quality
for Hydrogen (Moody's Maximized Analysis)
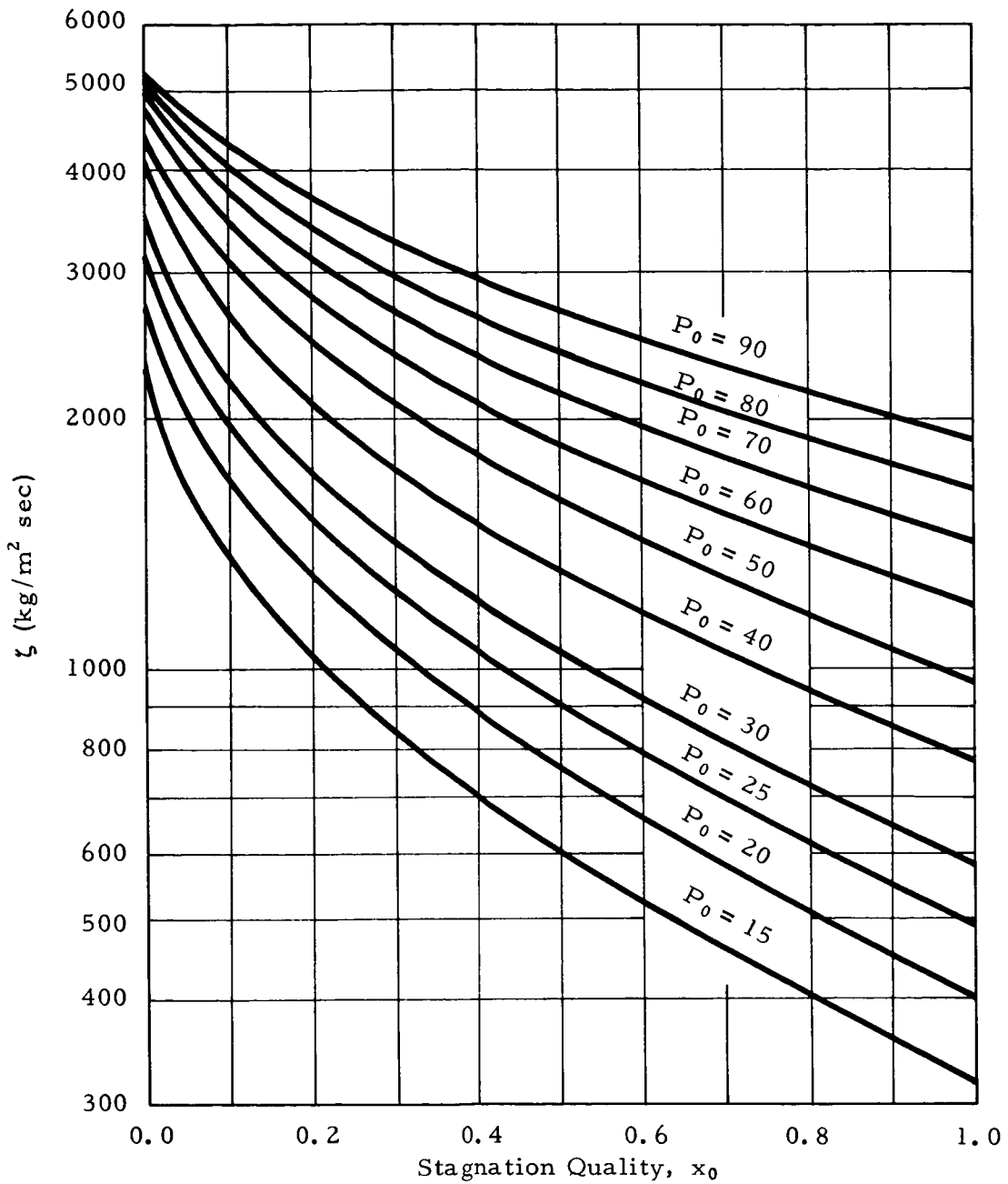
FIG 9   Critical Mass Flowrate Versus Stagnation Quality
         for Hydrogen (Moody's Maximized Analysis)
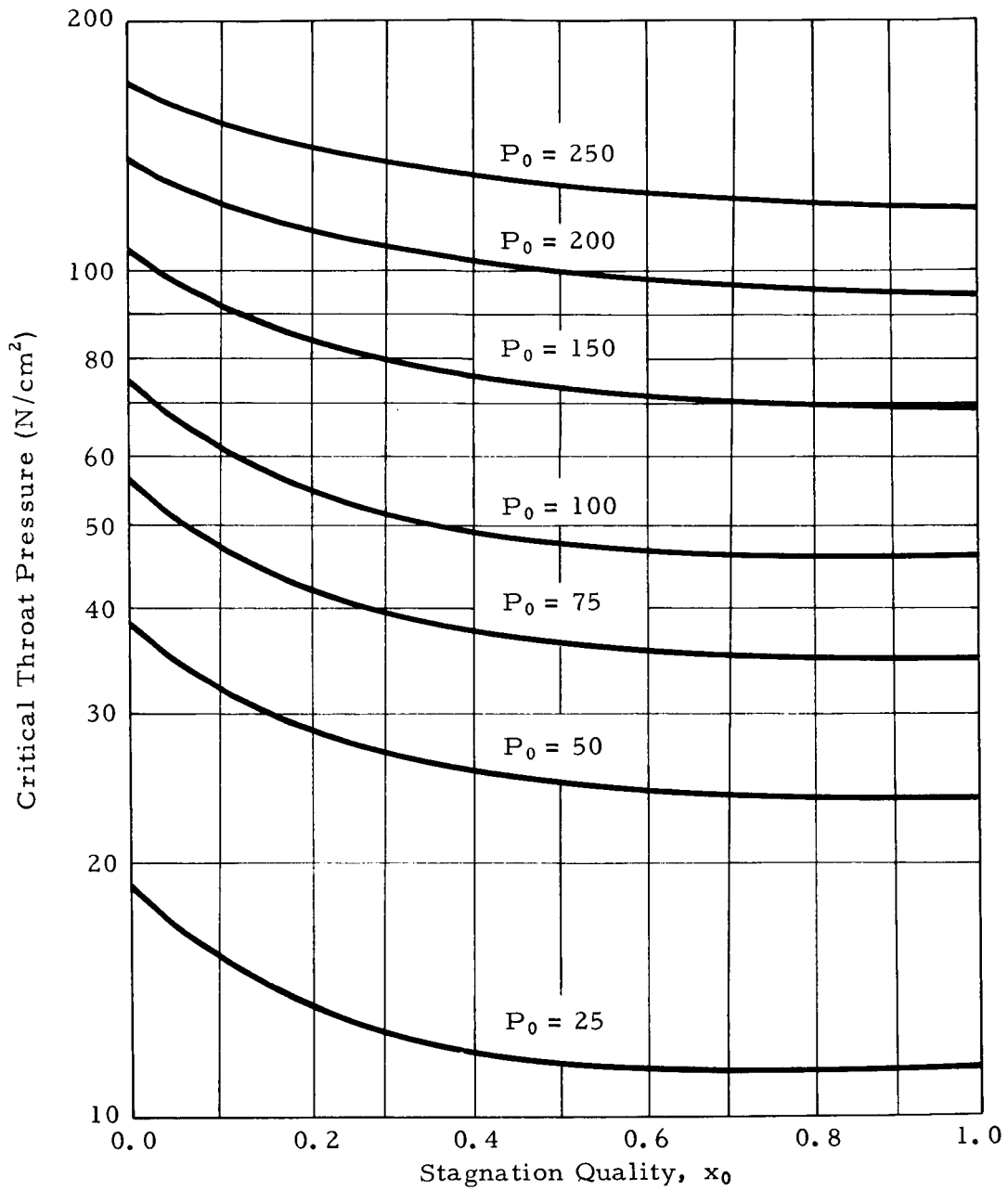
FIG 10   Critical Throat Pressure Versus Stagnation Quality
for Nitrogen (Moody's Maximized Analysis)
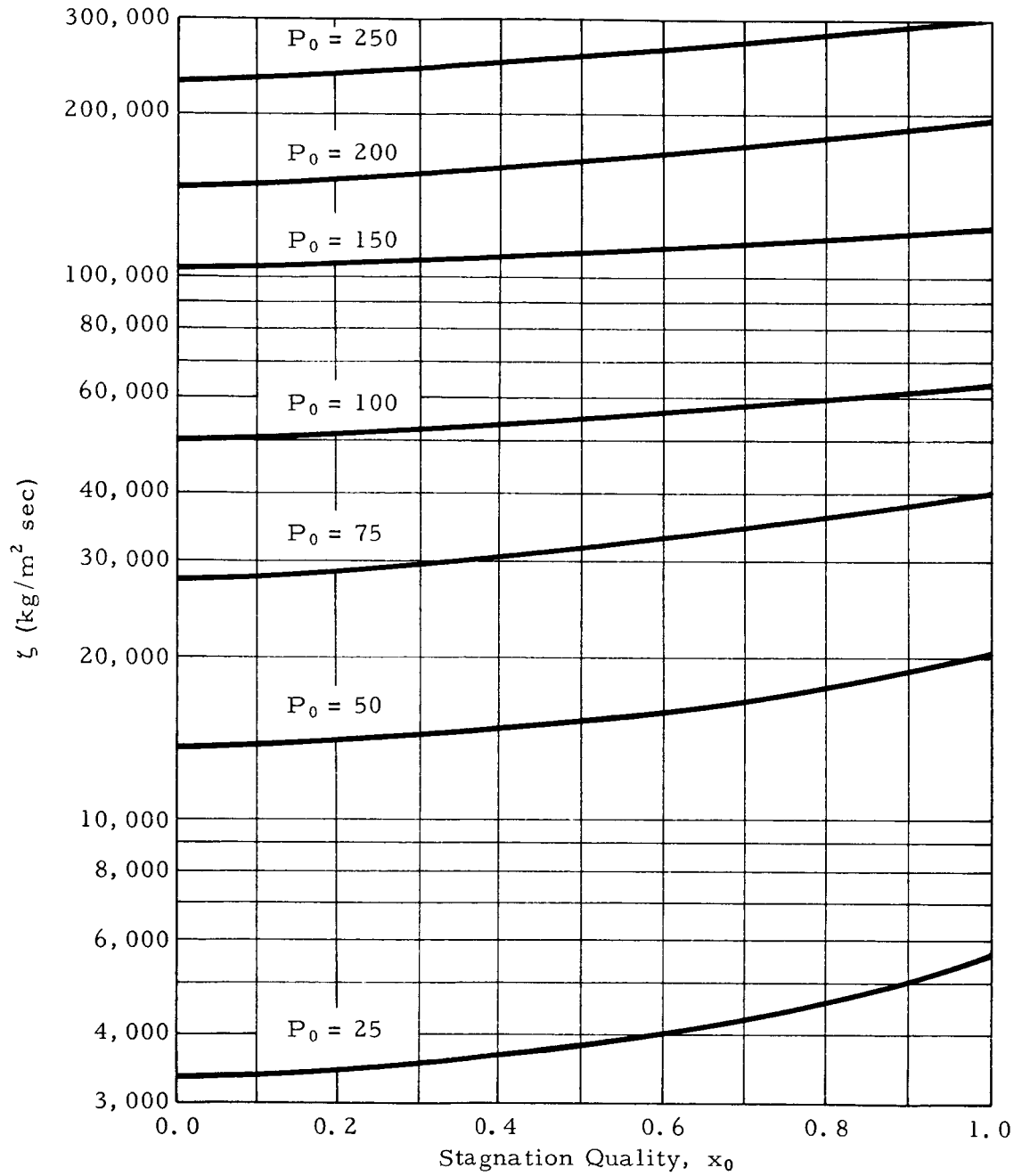
FIG 11   Critical Mass Flowrate Versus Stagnation Quality
for Nitrogen (Moody's Maximized Analysis)
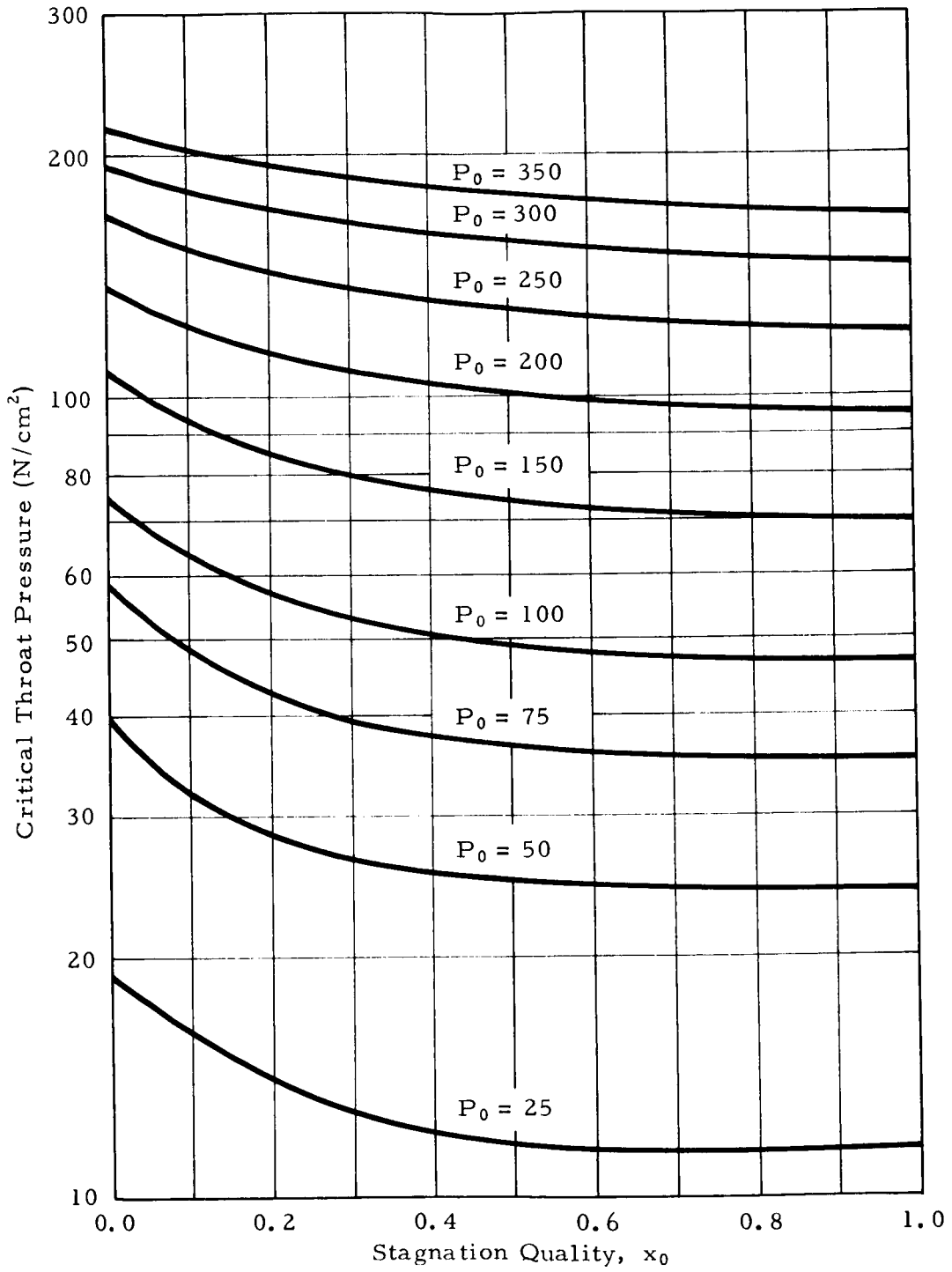
FIG 12   Critical Throat Pressure Versus Stagnation Quality
for Oxygen (Moody's Maximized Analysis)
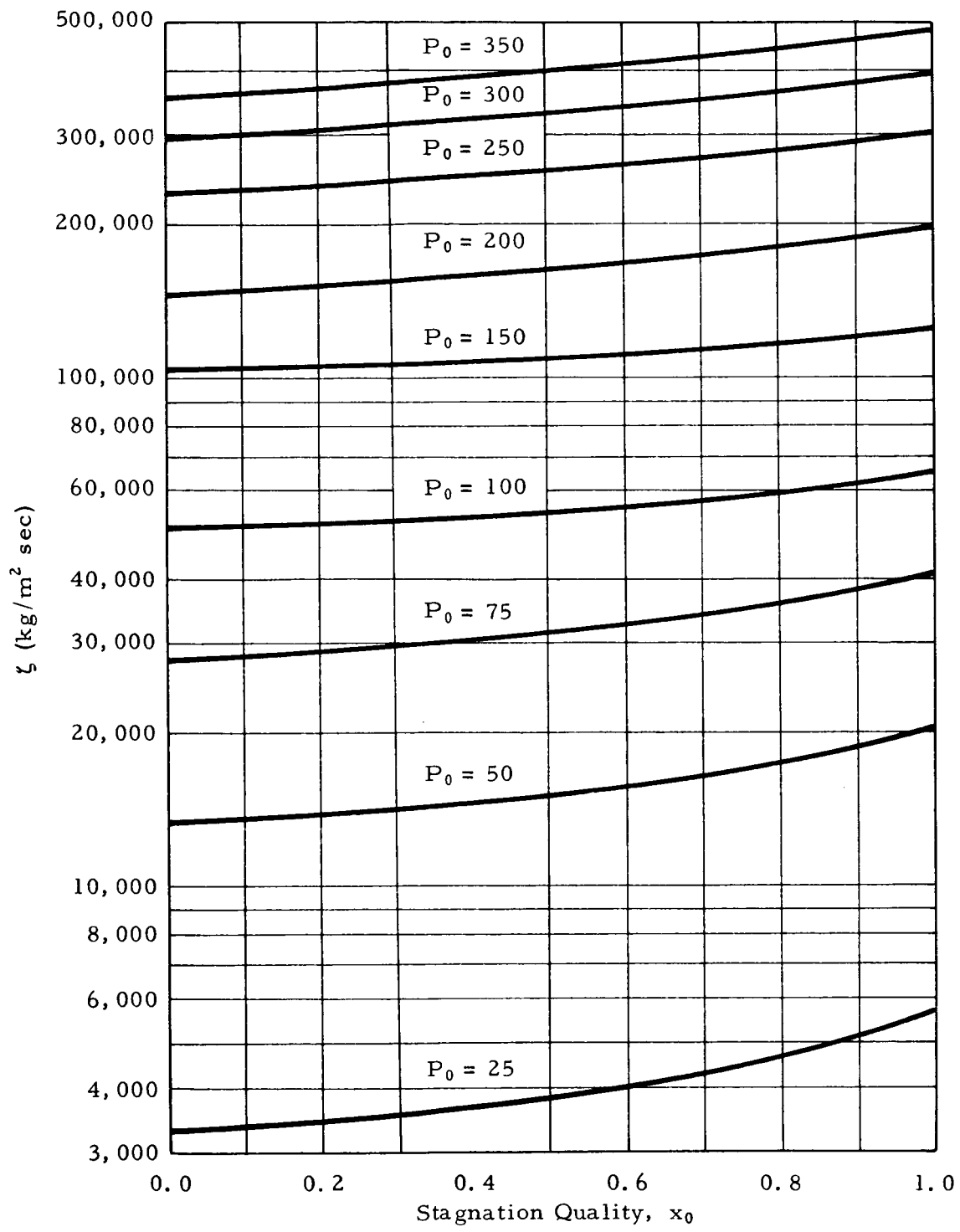
FIG 13   Critical Mass Flowrate Versus Stagnation Quality
for Oxygen (Moody's Maximized Analysis)
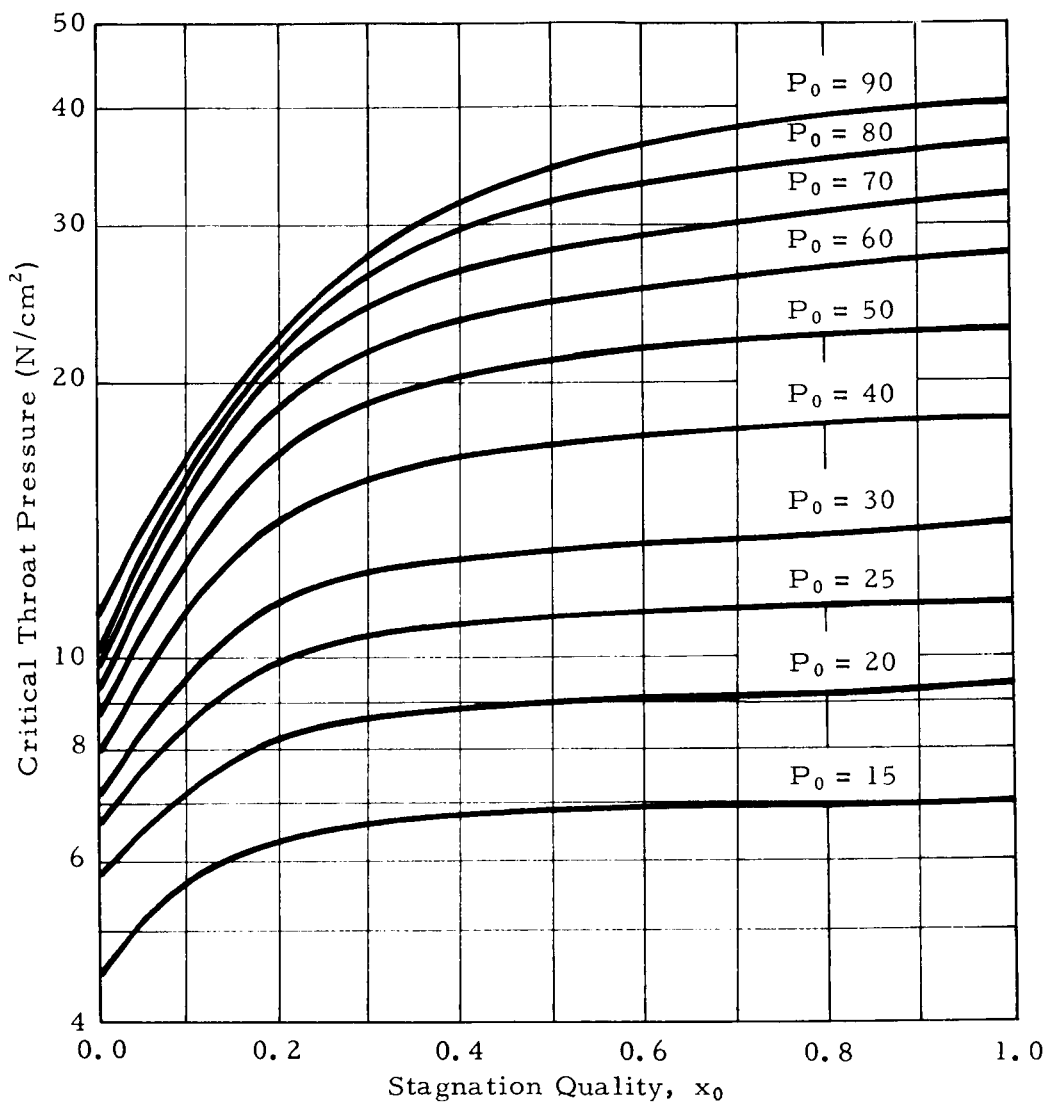
FIG 14   Critical Throat Pressure Versus Stagnation Quality
for Hydrogen (Ward's Frozen Equilibrium Model)
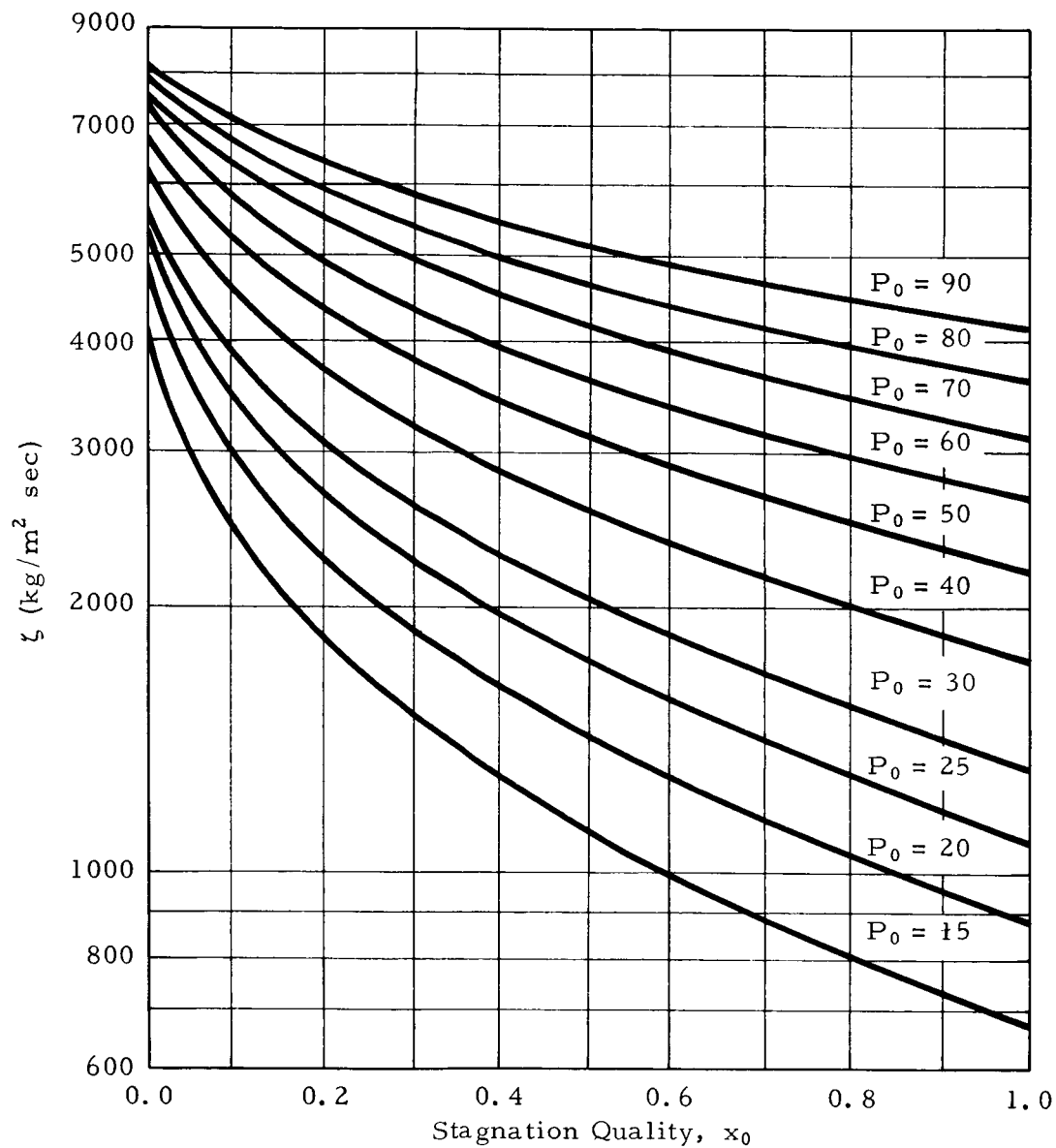
FIG 15   Critical Mass Flowrate Versus Stagnation Quality
for Hydrogen (Ward's Frozen Equilibrium Model)
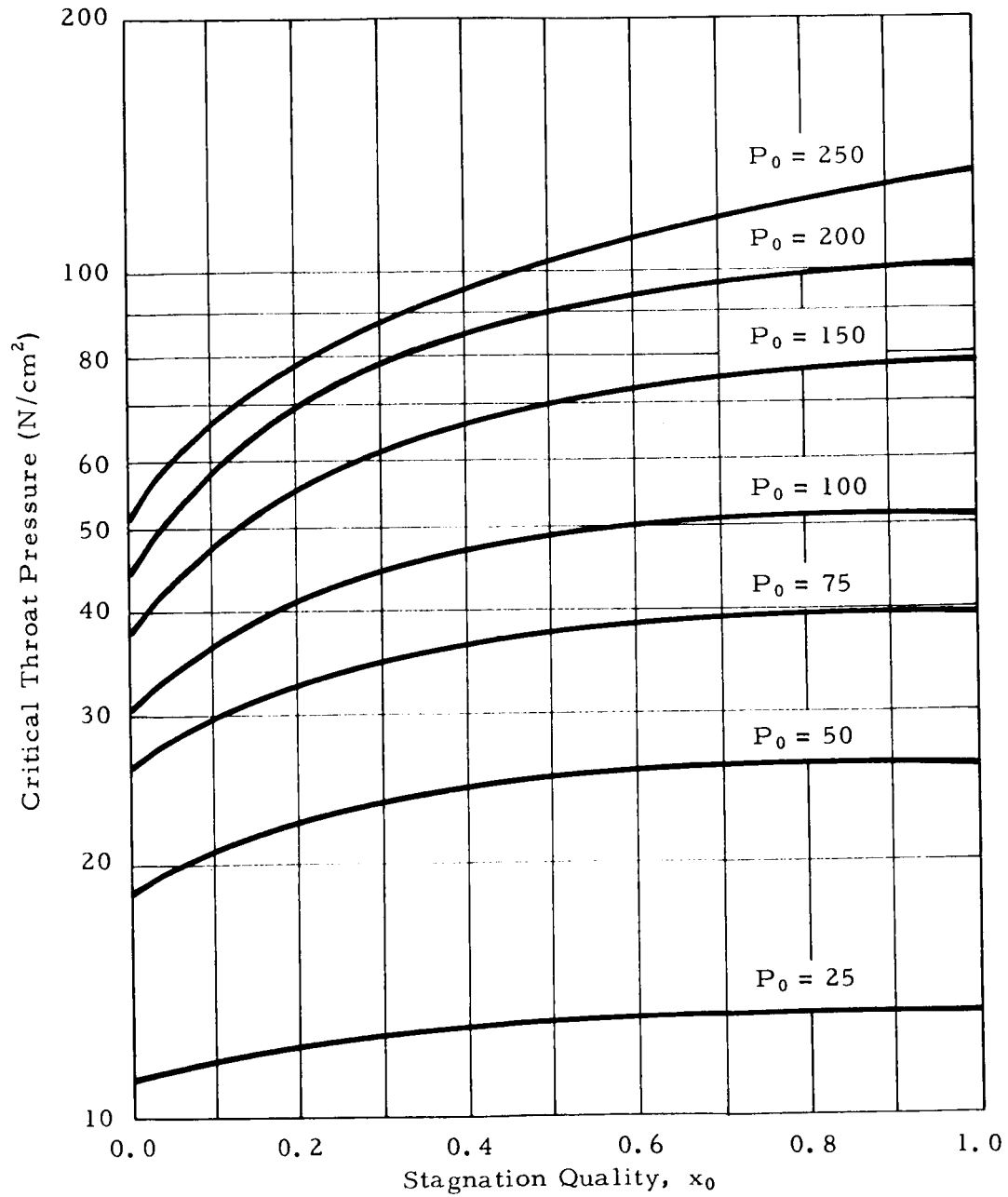
FIG 16   Critical Throat Pressure Versus Stagnation Quality
for Nitrogen (Ward's Frozen Equilibrium Model)
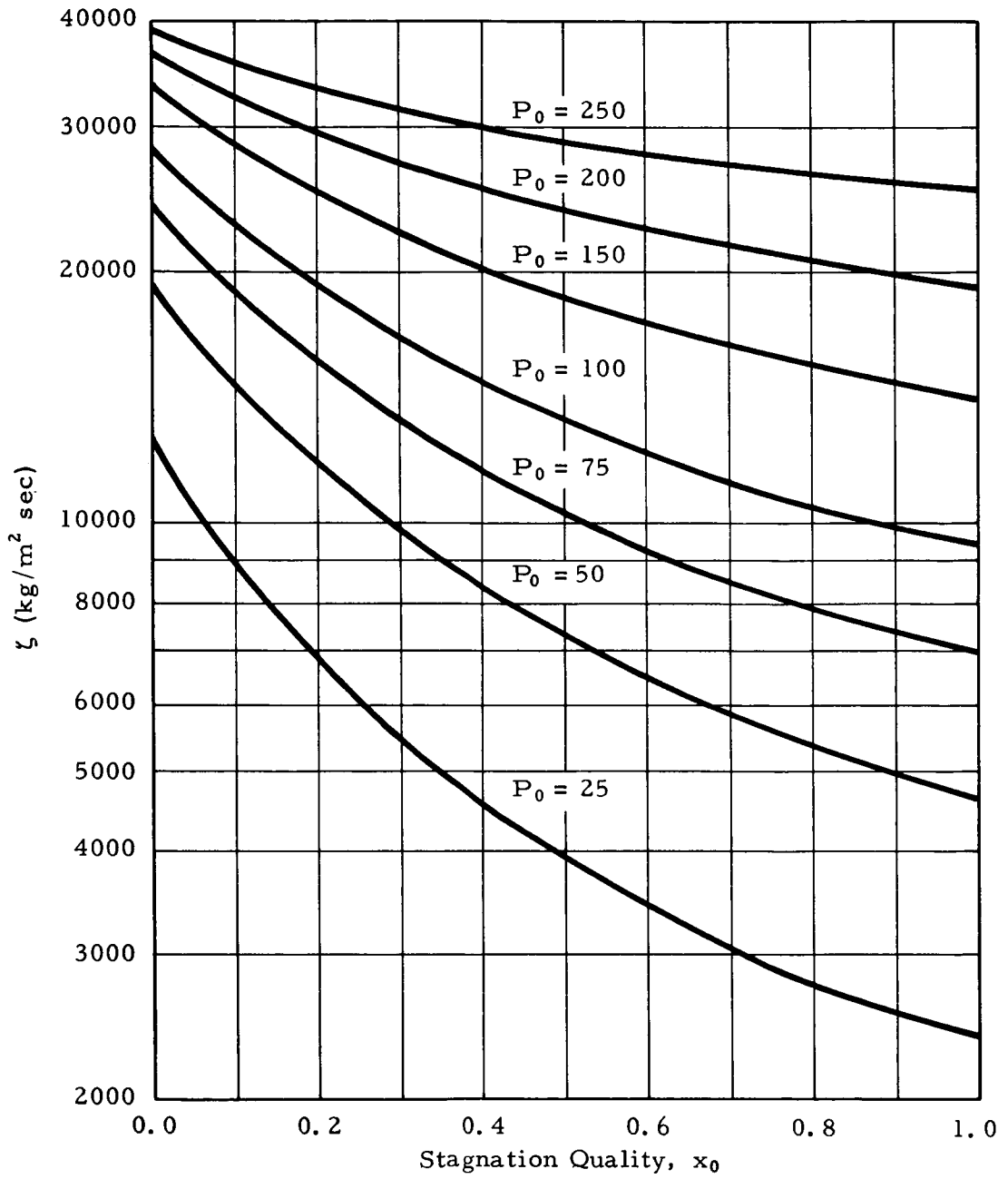
FIG 17   Critical Mass Flowrate Versus Stagnation Quality
for Nitrogen (Ward's Frozen Equilibrium Model)
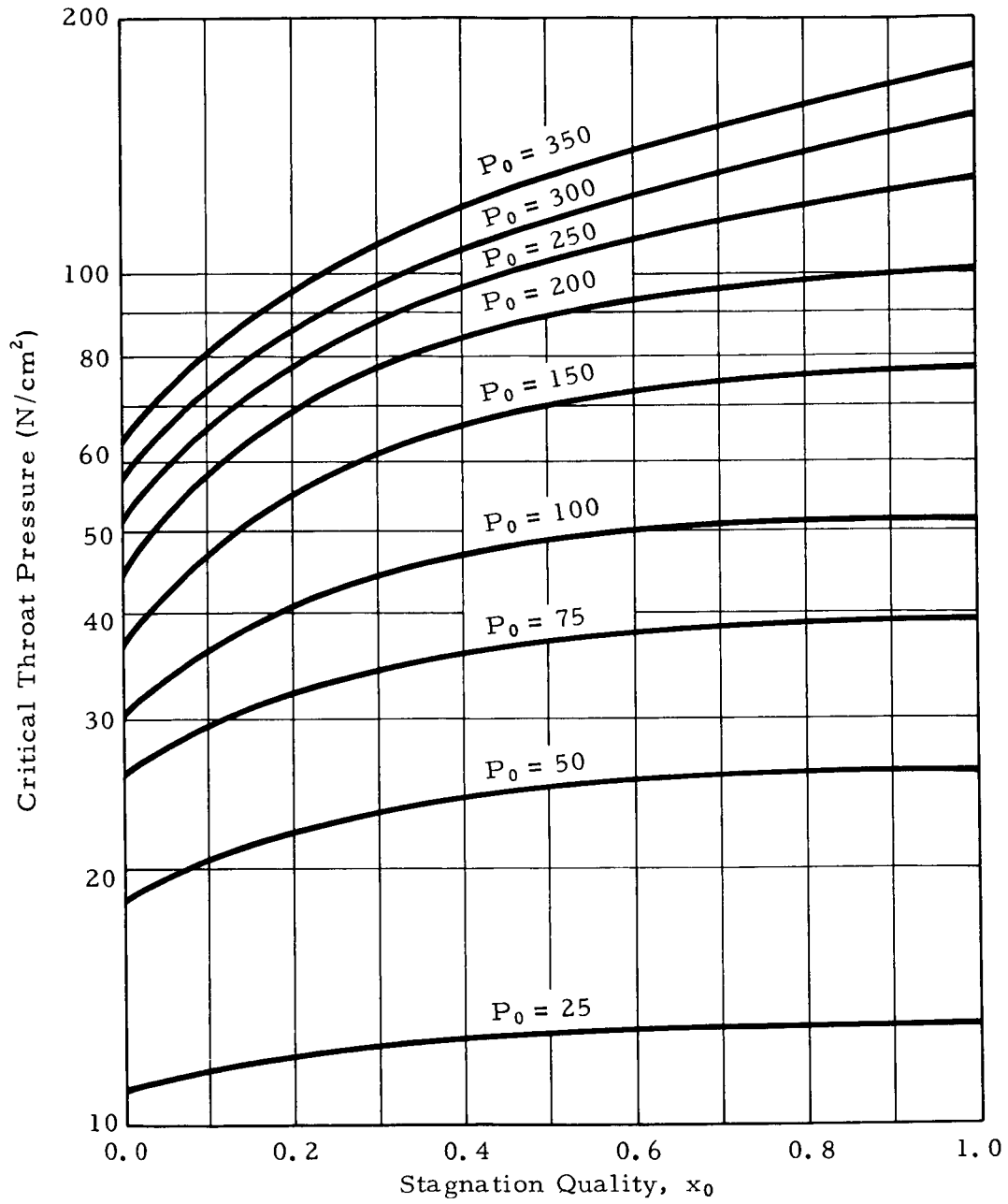
FIG 18   Critical Throat Pressure Versus Stagnation Quality
          for Oxygen (Ward's Frozen Equilibrium Model)

32
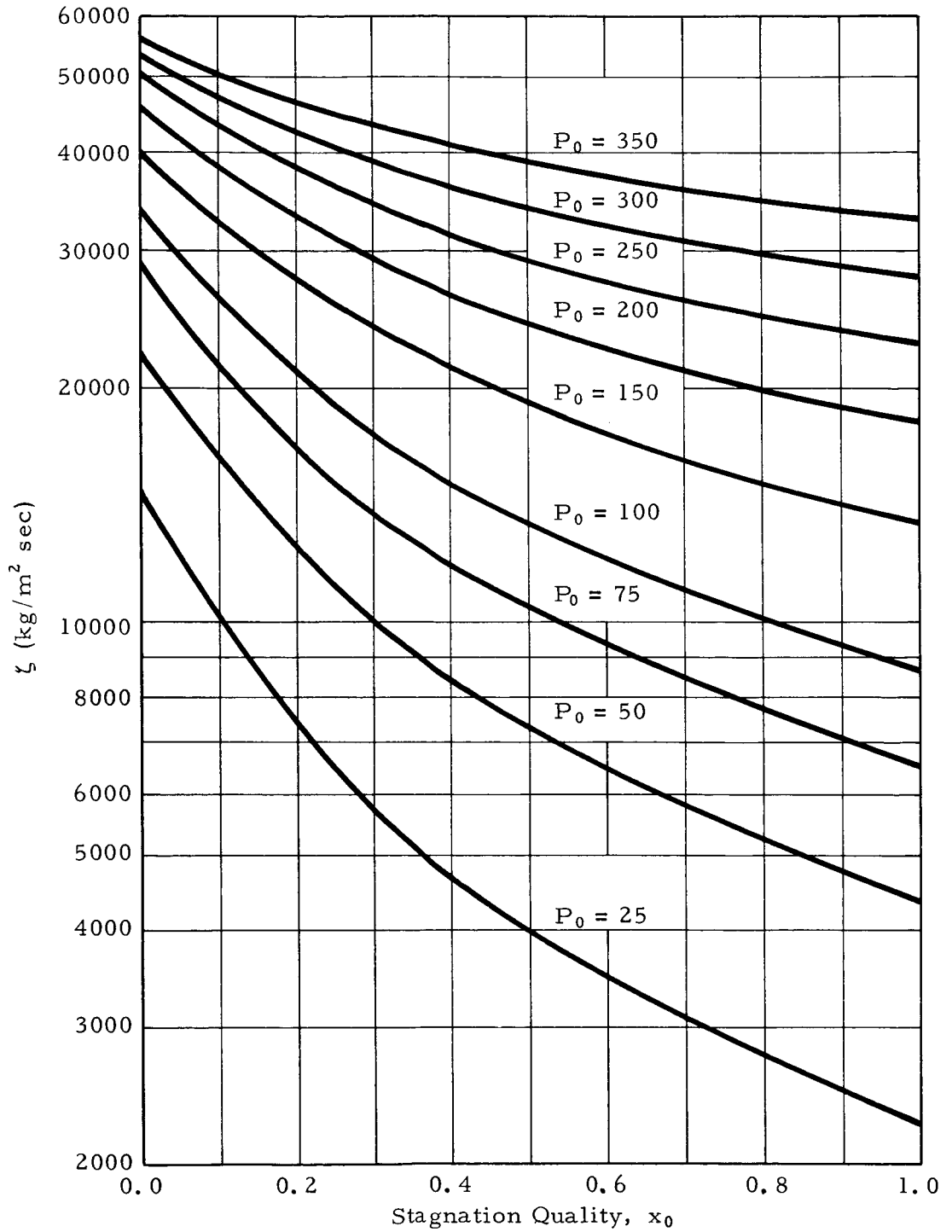
FIG 19   Critical Mass Flowrate Versus Stagnation Quality
for Oxygen (Ward's Frozen Equilibrium Model)
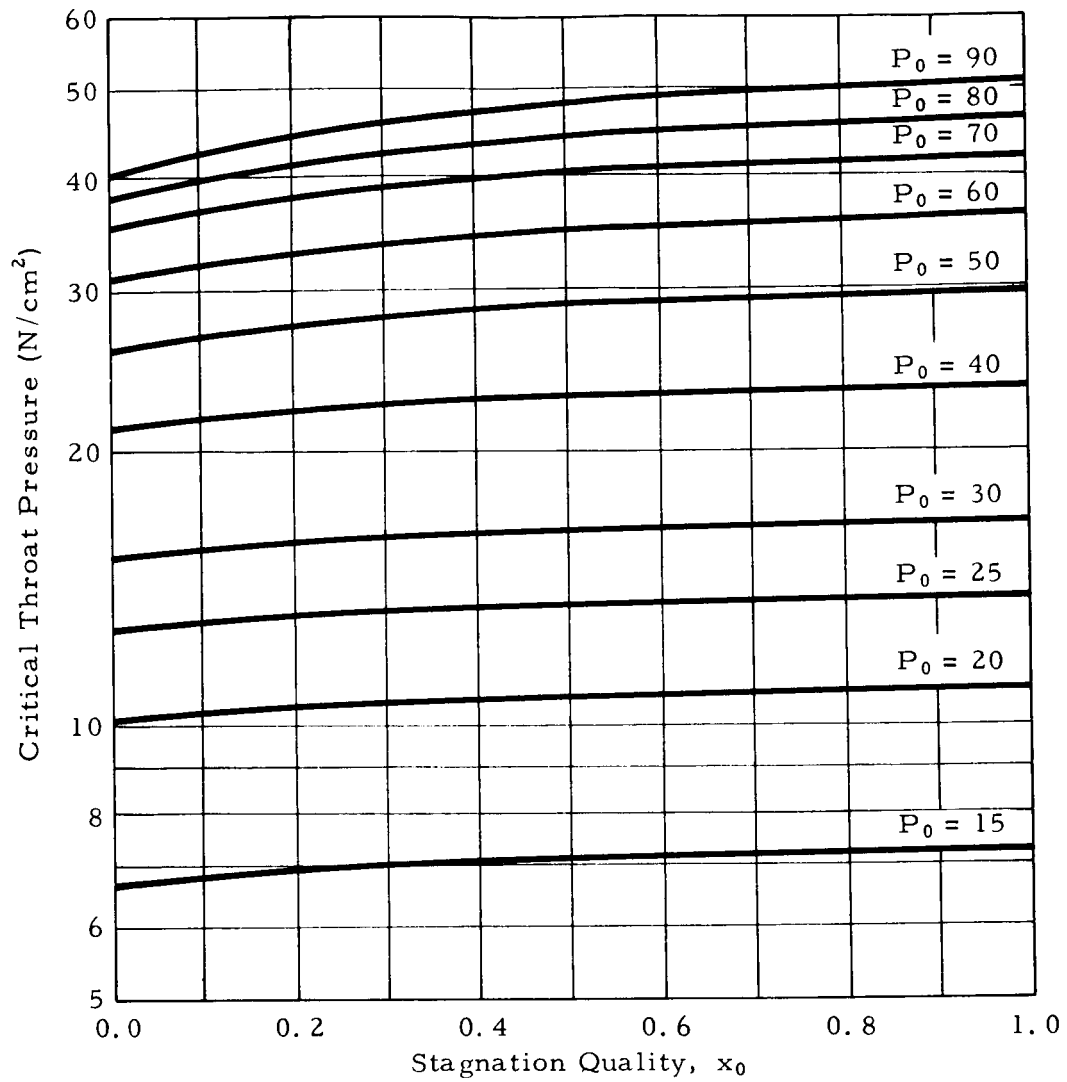
FIG 20   Critical Throat Pressure Versus Stagnation Quality
          for Hydrogen (Ward's Separate-Phase Shifting
          Equilibrium Model)
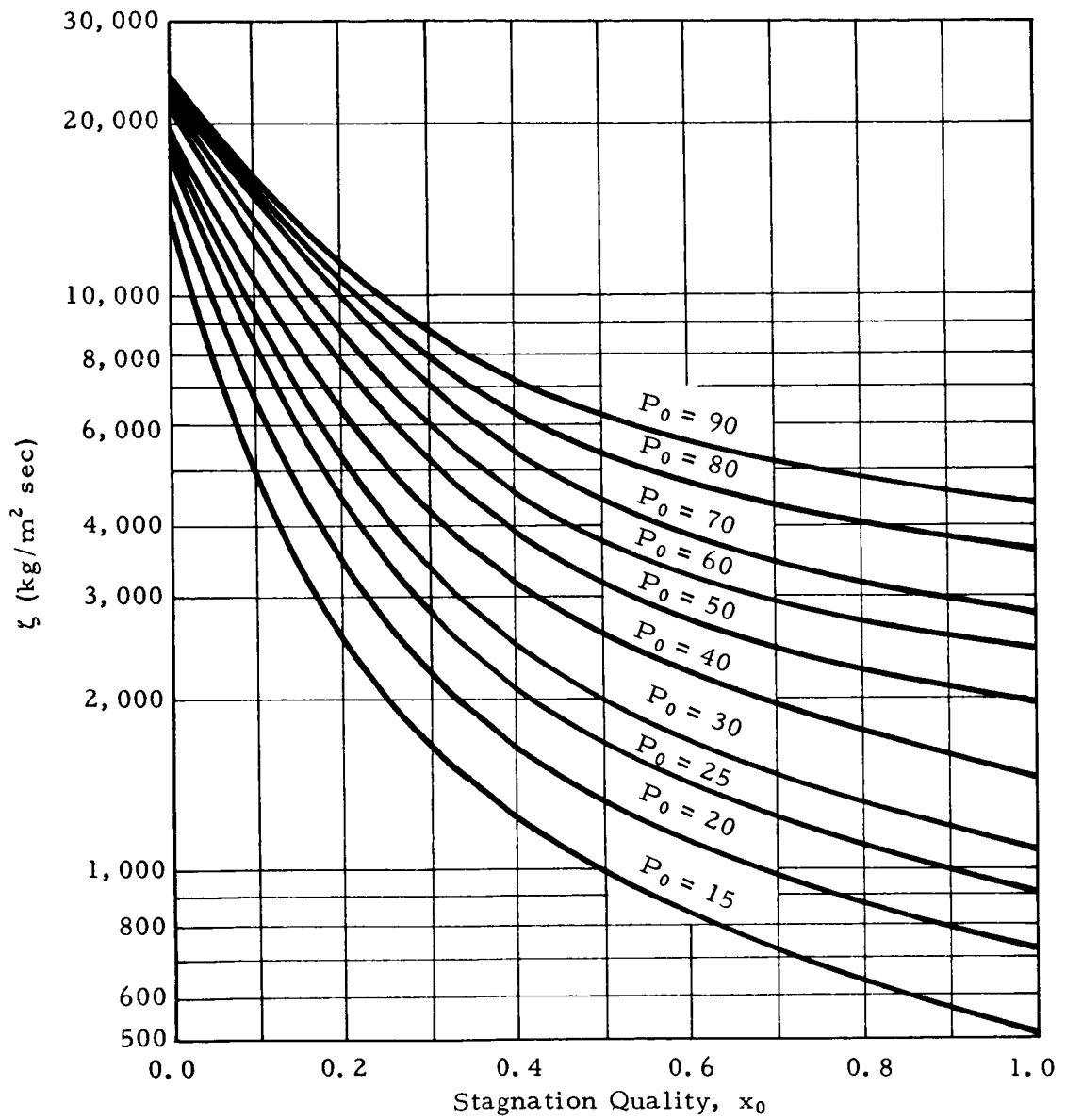
FIG 21   Critical Mass Flowrate Versus Stagnation Quality
for Hydrogen (Ward's Separate-Phase Shifting
Equilibrium Model)
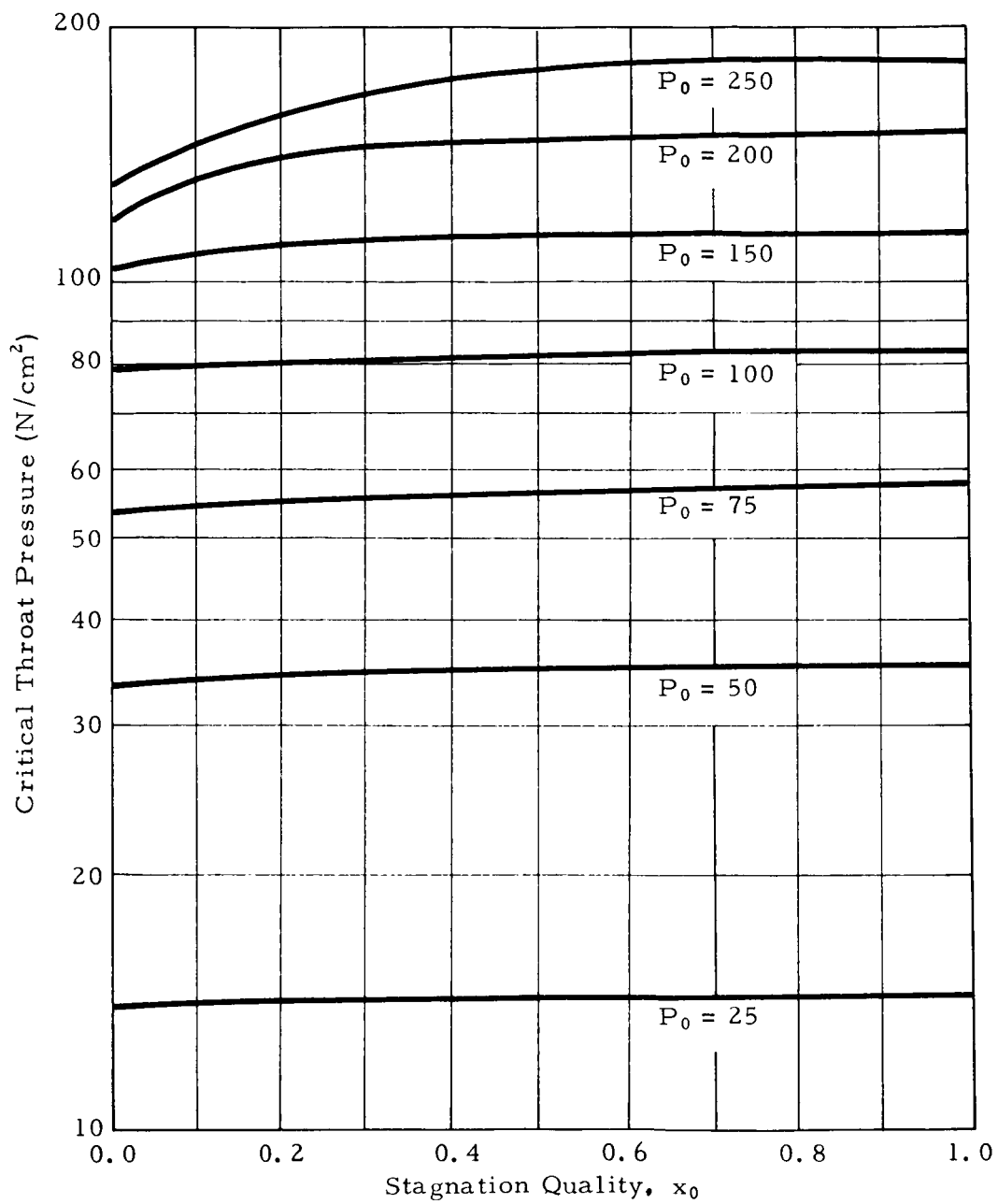
FIG 22   Critical Throat Pressure Versus Stagnation Quality
for Nitrogen (Ward's Separate-Phase Shifting
Equilibrium Model)
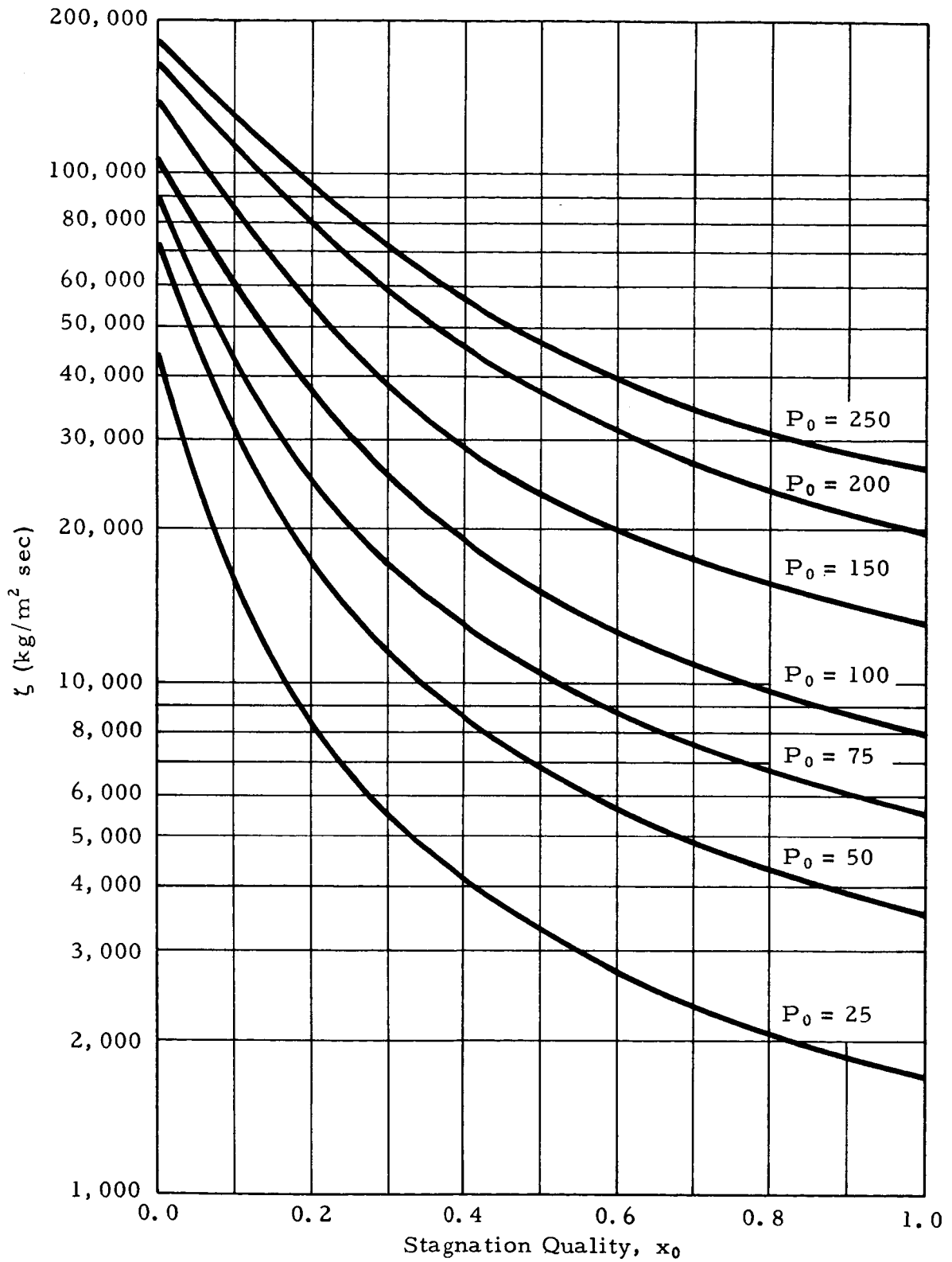
FIG 23   Critical Mass Flowrate Versus Stagnation Quality
for Nitrogen (Ward's Separate-Phase Shifting
Equilibrium Model)
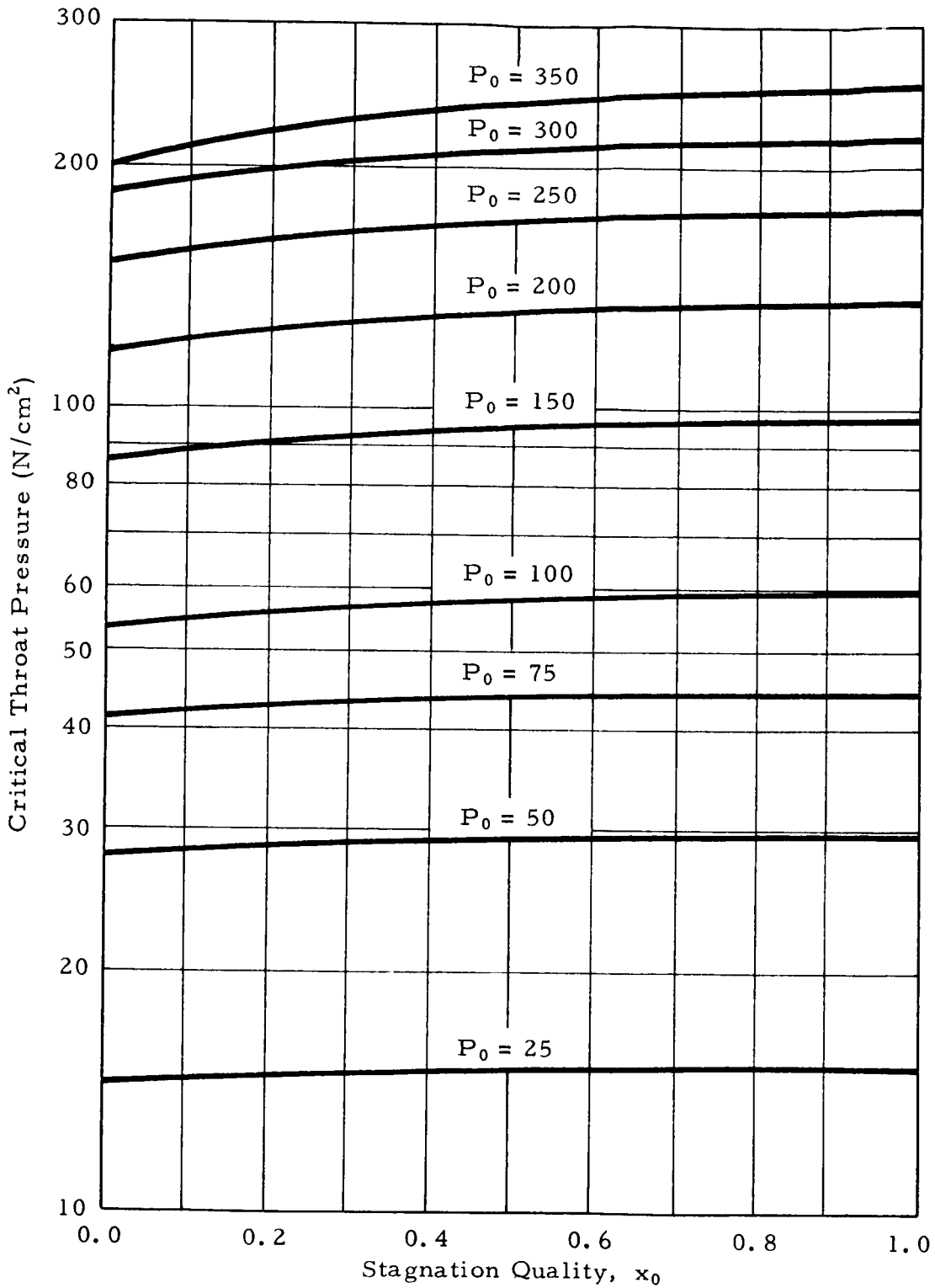
FIG 24   Critical Throat Pressure Versus Stagnation Quality
for Oxygen (Ward's Separate-Phase Shifting
Equilibrium Model)

38
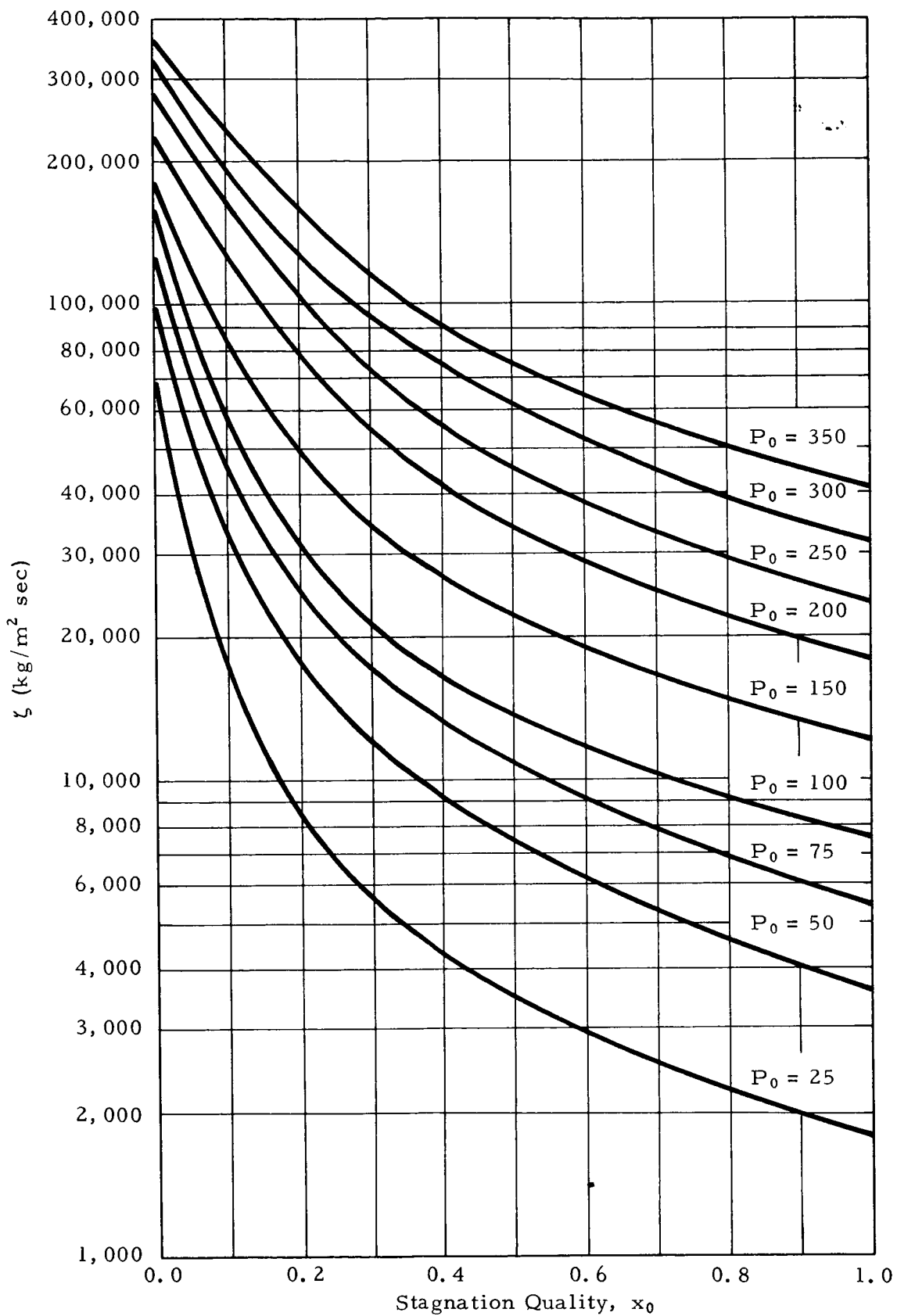
FIG 25 Critical Mass Flowrate Versus Stagnation Quality for Oxygen (Ward's Separate-Phase Shifting Equilibrium Model)
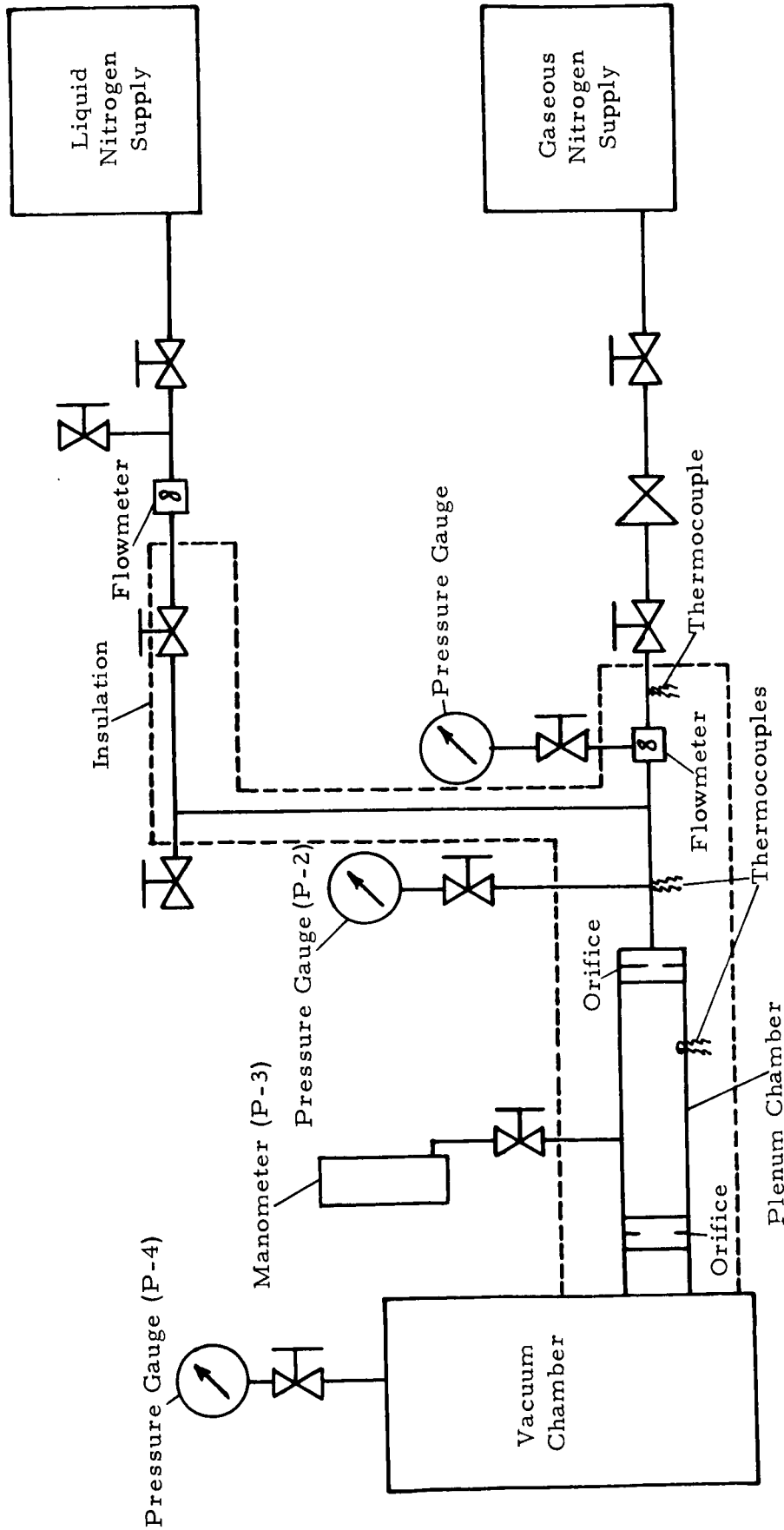
FIG 26   Experimental Apparatus Schematic
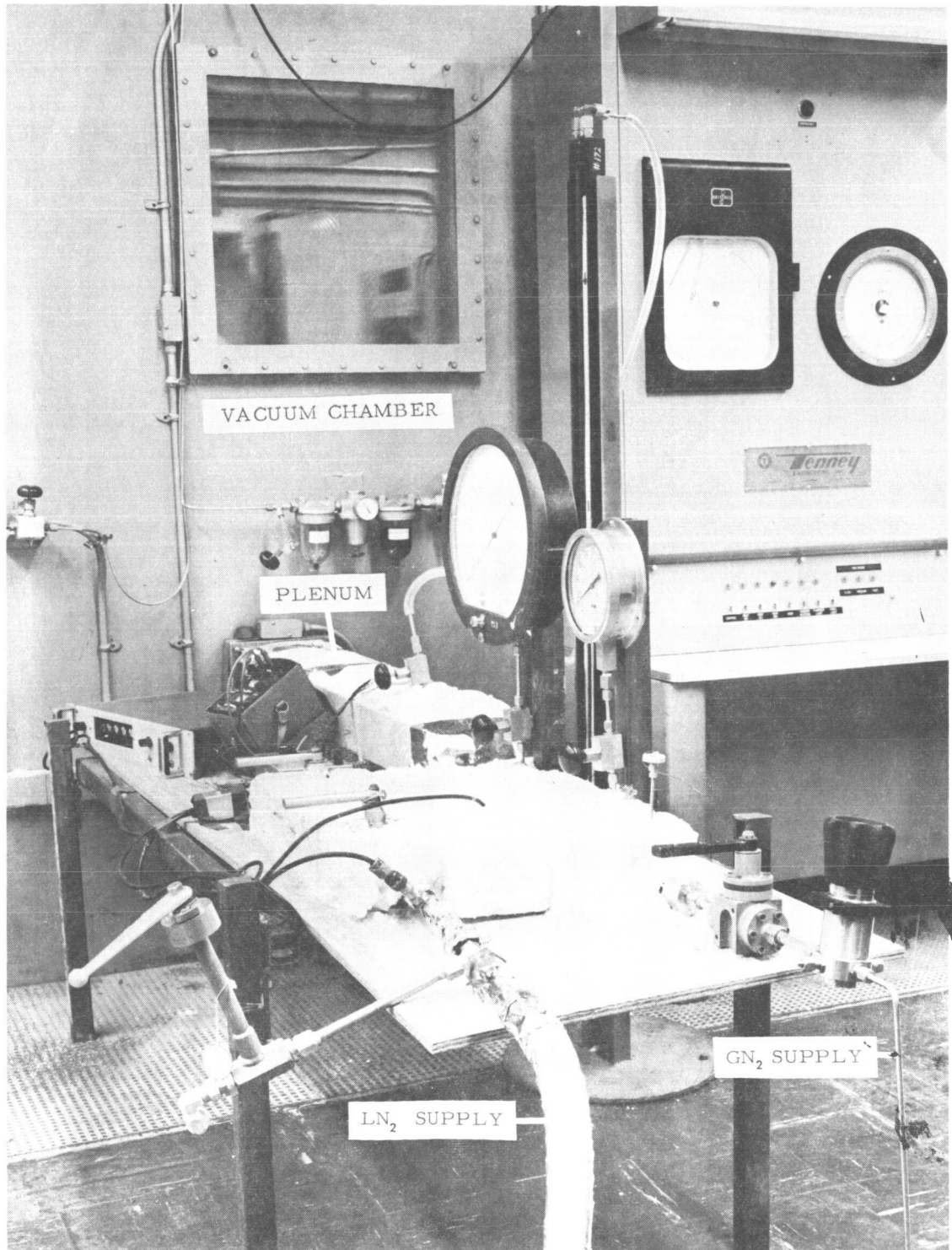
FIGURE 27 EXPERIMENTAL APPARATUS
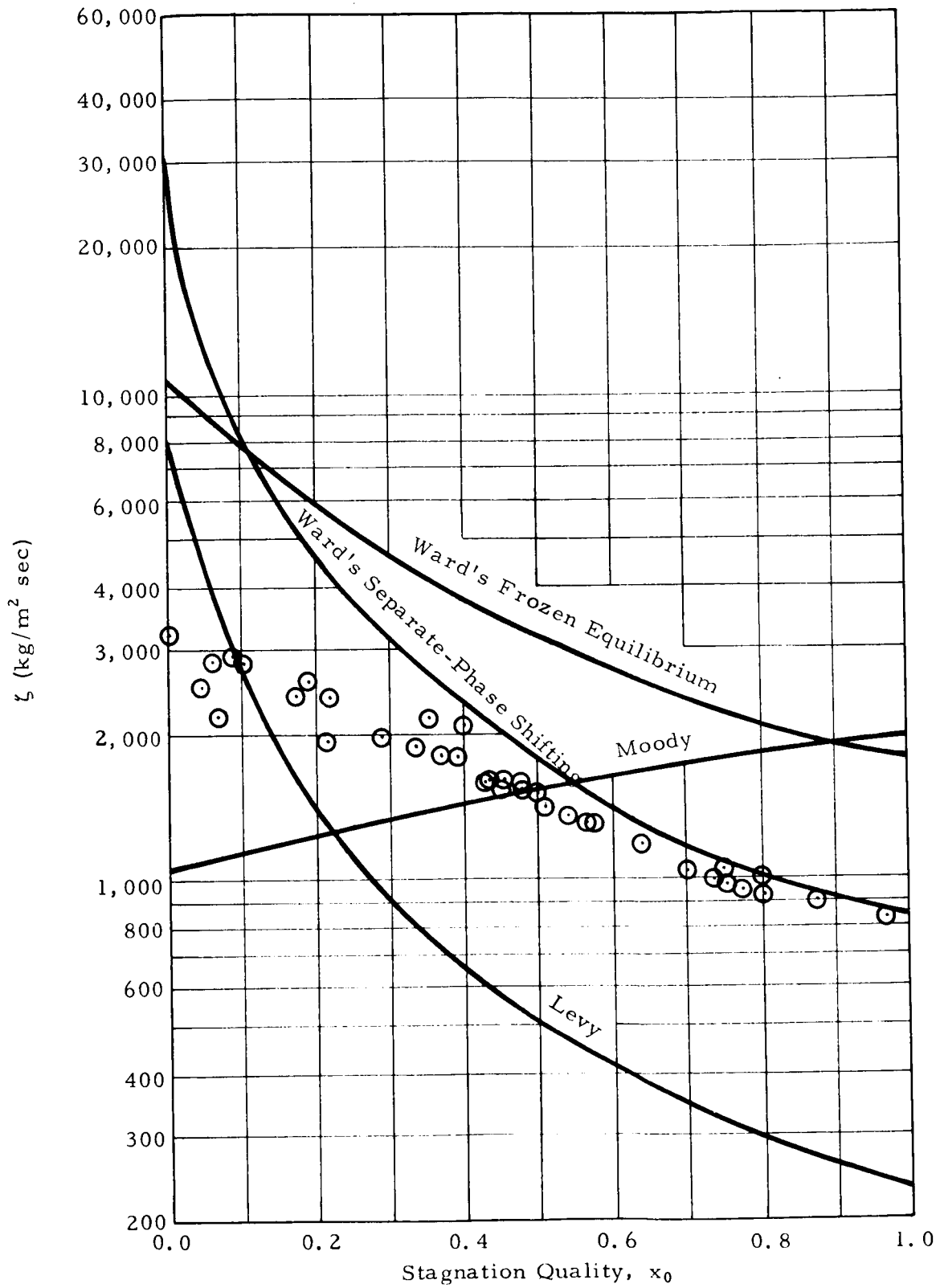
FIG 28   Comparison of Experimental Data to Predictions

CRITICAL FLOWRATE OF TWO-PHASE NITROGEN

By Hugh M. Campbell Jr. and Thomas J. Overcamp

The information in this report has been reviewed for security classification. Review of any information concerning Department of Defense or Atomic Energy Commission programs has been made by the MSFC Security Classification Officer. This report, in its entirety, has been determined to be unclassified.

This document has also been reviewed and approved for technical accuracy.

W. E. DICKSON
Chief, Propulsion Cryogenics Section

R. R. HEAD
Chief, Applied Mechanical Research Branch

H. G. PAUL
Chief, Propulsion Division

W. R. LUCAS
Director, Propulsion and Vehicle Engineering Laboratory

DISTRIBUTION

R-DIR   Mr. Weidner
R-ASTRO-DIR   Dr. Haeussermann
R-ASTRO-N   Mr. Moore
R-ME-DIR   Mr. Kuers
R-QUAL-DIR   Mr. Grau
R-RP-DIR   Dr. Stuhlinger
R-TEST-DIR   Mr. Heimburg
R-TEST-C   Mr. Halbrooks
R-TEST-T   Mr. Driscoll
R-TEST-SP   Mr. Pearson
R-P&VE-DIR   Dr. Lucas
R-P&VE-M   Mr. Kingsbury
R-P&VE-S   Mr. Kroll
R-P&VE-V   Mr. Aberg
R-P&VE-P   Mr. Paul
R-P&VE-P   Mr. McCool
R-P&VE-PA   Mr. Thomson
R-P&VE-PE   Dr. Head   (25)
R-P&VE-PM   Mr. Fuhrmann
R-P&VE-PP   Mr. Heusinger
R-P&VE-PT   Mr. Wood
R-P&VE-PT   Mr. Worlund
R-P&VE-PT   Mr. Helms
R-P&VE-PR   Mr. Eby
R-P&VE-RT   Mr. Hofues
MS-IP   Mr. Remer
MS-H   Mr. Akens
K-DIR   Dr. Debus
MS-T   (6)
CC-P
I-RM-M
MS-IL (8)

Scientific and Technical Information Facility   (25 copies)
Attn: NASA Representative (S-AK/RKT)
P. O. Box 33
College Park, Maryland 20740

Defense Documentation Center   (20 copies)
Cameron Station
Alexandria, Virginia 22314